LBL-37677
UC-410
Preprint

Lawrence Berkeley Laboratory
UNIVERSITY OF CALIFORNIA

Accelerator & Fusion Research Division

Submitted to Journal of the Optical Society of America

X-Ray Holographic Microscopy via Photoresist Recording and Atomic-Force Microscope Readout

S. Lindaas, M. Howells, C. Jacobsen, and A. Kalinovsky

August 1995

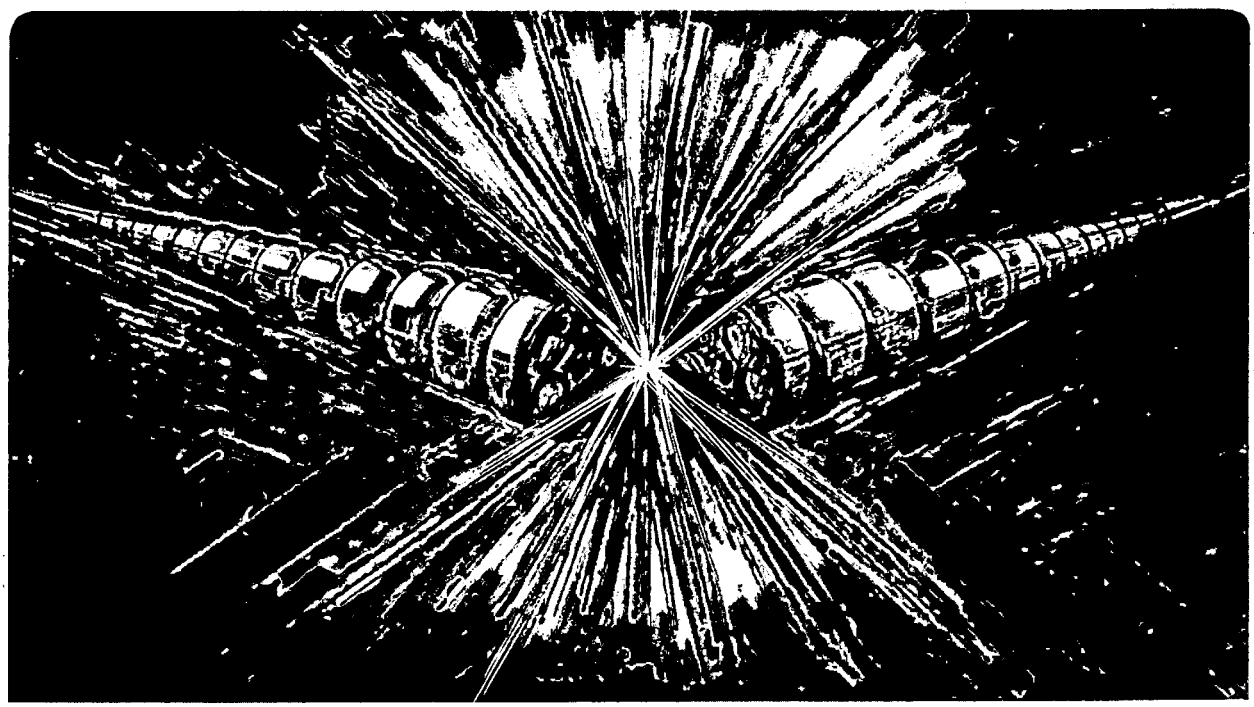

Prepared for the U.S. Department of Energy under Contract Number DE-AC03-76SF00098

DISCLAIMER

LBL-37677
LSBL-278
UC-410

X-RAY HOLOGRAPHIC MICROSCOPY VIA PHOTORESIST RECORDING AND ATOMIC-FORCE MICROSCOPE READOUT*

S. Lindaas and Malcolm Howells
Advanced Light Source
Accelerator and Fusion Research Division
Lawrence Berkeley Laboratory
University of California
Berkeley, CA 94720, USA

Chris Jacobsen and Alex Kalinovsky
Department of Physics
State University of New York
Stony Brook, NY 11794-3800

*This work was supported by the Director, Office of Energy Research, Office of Basic Energy Sciences, Materials Sciences Division, of the U.S. Department of Energy, under Contract No. DE-AC03-76SF00098.

1 Introduction

1.1 History

The basic ideas of holography were put forward in 1948 by D. Gabor as part of the search for atomic-resolution electron microscopy [Gabor 1948]. At that time, the invention of the laser was still several years away, so Gabor made an experimental demonstration using visible light. Four years later the application of the holographic principle to x-ray imaging was suggested by Baez [Baez 1952]. Considerable effort was made around that time to record x-ray holograms using a point-focus x-ray tube and photographic film [El-Sum 1952]. The intention was to reconstruct the image with visible light and thereby achieve magnification without having to build an x-ray lens. However, the task proved difficult and it was some years before reconstructed images of even the simplest objects were obtained [Giles 1969, Aoki 1974]. It became clear that, for effective x-ray holographic microscopy, new technology would be needed and interest in the method diminished.

With a modern perspective we understand that the x-ray tubes had insufficient coherent power and the film had inadequate resolution. Thus, when the prospect of x-ray laser and synchrotron radiation sources with many orders of magnitude more coherent power appeared in the early nineteen eighties, interest in x-ray holography revived [Solem 1982, Howells 1984]. Experimental programs were started at various centers [Howells 1986, Howells 1987, Joyeux 1988a] leading to the first achievement of submicron-resolution reconstructed images at Brookhaven [Jacobsen 1988, Jacobsen 1990b] and Orsay [Joyeux 1988b] and the demonstration of x-ray laser holography at Livermore [Trebes 1987]. The history of these efforts has been reviewed by Jacobsen [Jacobsen 1990a].

1.2 Motivation

The original motivation for doing holography with x-rays was the desire to construct an x-ray microscope without having to build an x-ray lens. Even though we now have Fresnel-zone-plate x-ray lenses, this concept is of interest since the best (highest-resolution) lenses have efficiencies of only a few percent and a high level of capital investment and technical skill is required to make them. We may list our other motivations as follows:

- The type of in-line holography that we are using encodes both the amplitude- and phase-contrast images simultaneously.
- The resolution of in-line holography is set by the ability of resist to record high-frequency x-ray interference fringes. We believe that ultimately this may allow higher resolution imaging than the alternative methods based on using the same resist to write and manufacture zone plates.
- There is no need to focus a holographic exposure so that holography is well-suited to imaging with fast-pulse x-ray sources. If the pulse is fast enough [Solem 1986, London 1989, London 1992], the image information can be captured before radiation damage has time to occur so this provides a way to avoid damage at room temperature. Suitable pulsed x-ray sources based on x-ray lasers and free-electron lasers are under development at several laboratories. Consequently we view our development of x-ray holography using synchrotron radiation as part of our preparation for exploiting those sources in the future.

- X-ray holography experiments are exceedingly easy: one just exposes the resist through the sample, which can be anywhere in the roughly $1\,\mathrm{mm}^2$ area illuminated by the beam in the present experiments. This simplifies a number of sample treatments including the construction of a cryo-imaging setup.

Another line of reasoning concerns the general advantages of practicing microscopy with soft x-rays in the spectral region $1.0 - 5.0\,\mathrm{nm}$, particularly in the range between the oxygen K edge (2.38 nm) and the carbon K edge (4.37 nm). Within the latter range, materials of all kinds, especially biological specimens, can be imaged in water with good absorption contrast up to a total thickness of several microns. The use of phase contrast [Rudolph 1990] extends these advantages to even thicker water layers and a somewhat wider spectral range. The technology and applications of x-ray microscopy have been described in several recent review articles [Kirz 1995, Michette 1988] and conference proceedings [Michette 1992, Aristov 1994, Jacobsen 1992b]. X-ray holography is, in essence, a member of this wider family of x-ray microscopes. It shares the simplicity of the x-ray contact printing technique (x-ray microradiography), and the amplitude- and phase-contrast capability of transmission and scanning transmission x-ray microscopes. However, while holography has in principle the capability to map chemical elements and determine their chemical bonding states, this is much easier to do in practice using a scanning transmission x-ray microscope.

The three-dimensional imaging capabilities of these x-ray techniques are limited by the same information-theory constraints that apply to all types of imaging and which mandate a multiplicity of views. One should not be deceived by the vivid three-dimensional images observed using visible-light holography. These normally reveal only the shapes of the outer surfaces of solid objects, not their internal features. Moreover, such images require a high numerical-aperture geometry during hologram recording and still deliver resolution which is far below the diffraction limit. In x-ray holography we do wish to see internal features, we do not have high numerical aperture and we do desire diffraction-limited resolution. Thus, for most purposes, to achieve three-dimensional images the tomographic method with multiple views is required in x-ray holography just as much as in other types of x-ray imaging [Joyeux 1989a].

1.3 Starting point for the present work

The method by which the present authors first demonstrated sub-micron resolution x-ray holographic microscopy [Jacobsen 1990b], was based on the following sequence of operations: (*i*) record the hologram in resist spun on a soft-x-ray-transparent membrane (120 nm-thick silicon nitride), (*ii*) liquid develop the resist leading to a representation of the hologram fringes by surface relief, (*iii*) glancing-incidence shadow the surface with heavy metal, (*iv*) image the metal distribution onto a photographic plate using a transmission electron microscope at low magnification, (*v*) digitize the plate with a microdensitometer and (*vi*) calculate the final image by digital image processing.

This procedure was essentially a laboratory demonstration and, although it produced good images, it was slow, complex, nonlinear and vulnerable to beam damage and optical aberrations in the electron microscope. The process of recording the hologram using a soft x-ray undulator (see Section 7.1) was the most straightforward part of the process. It involved placing the sample or samples in the x-ray beam and taking an exposure of one to a few minutes. On the other hand the process of recovering the image from the recorded hologram required considerable time and carried risks of losing or corrupting the information. For routine use in scientific investigations a simpler

method of hologram readout with greater accuracy and fewer steps would be required. We now have such a method and we describe it in detail in what follows.

1.4 Definition of the subject matter for this paper

In this paper we describe the basis for our choice of in-line (Gabor-type) geometry for our x-ray holographic microscopy system. We outline the technical requirements for such a system to work with good resolution with particular attention to the question of hologram readout and we describe how we have addressed the readout problem by means of a specially-developed atomic-force microscope (AFM). We explain why it was necessary to build a custom AFM, and we give a description of its construction and performance characteristics. We give a brief account of how an x-ray holography experiment is done and show examples of how the data from such an experiment are read by the AFM and used to produce reconstructed images by digital image processing.

We discuss the contribution that holography, practiced in this new way, can be expected to make to biological investigations in the future with special reference to the question of radiation damage. We argue on the basis of evidence from electron microscopy that imaging at cryogenic temperatures promises to allow sufficient applied dose to permit a full tilt series and tomographic reconstruction of a three-dimensional image without the creation of radiation artifacts at the resolution level where soft x-ray holography can operate.

2 Holographic geometries

2.1 In-line holography

The original holographic experiment of Gabor utilized an on-axis reference wave (the basic geometry is sketched in Figure 1). The scheme is particularly simple and can be implemented without any optics other than the source and the recording medium. With a high resolution detector and the means to read it one should, in principle, realize an image resolution about the same as that of the detector, as originally predicted by Baez [Baez 1952]. The main limitation of in-line holography is that the object field must have high overall transparency to provide a good reference beam from the transmitted light. A further disadvantage is the so-called twin-image artifact. Assuming a reconstruction using the original reference wave, the fringes recorded in the hologram diffract the reconstructing light beam equally into the plus and minus first orders in such a way that two images are formed: one, a virtual image, at the sample position and the other, a real image, at a distance z (Figure 1B) downstream of the hologram. The light from these two images is mingled and there is no simple way to achieve a separation. At the plane of the real image, the light diverging from the virtual image at S in Figure 1B interferes with the light in the zero-order (undiffracted) beam to produce a second hologram mixed with the real image. The fringes from this unwanted hologram can be seen in Figures 8 and 10. We discuss ways to address this problem later.

2.2 Off-axis holography

In visible-light optics the traditional solution to the twin image problem is to use an off-axis reference beam [Leith 1962] which is particularly well suited to laser sources. However, from the point of

view of high-resolution holographic imaging with x-rays, the twin-image advantage of the off-axis technique is overwhelmed by its disadvantages. To achieve angular (*i.e.* frequency-space) separation of the image-bearing signals from each other and from the intermodulation signal, one must settle for a resolution which is worse than that of the recording medium (and hence also than that of an in-line hologram) by a factor of 4 [Collier 1971]. In addition, the coherence-length requirement is substantially increased compared to the in-line geometry and a requirement for some type of beam splitter (with difficult manufacturing tolerances) is introduced.

2.3 Fourier-transform x-ray holography

If the reference source (say a point) is placed close to the object then the reference and object beams will interfere at a small angle leading to low-frequency fringes [Stroke 1964, Reuter 1976]. Such fringes can be recorded by a relatively low-resolution detector such as a charge-coupled device connected to a computer. This brings many advantages in rapid return of the reconstructed image and freedom from twin-image problems as demonstrated by McNulty *et al.* [McNulty 1992a, McNulty 1992b]. The tradeoff is that the experiment is no longer simple and optics-free and the resolution is limited by that of the optics forming the reference point source. For the experiments reported here we placed highest priority on resolution and chose the in-line geometry. It may be that photoresist will ultimately deliver better resolution with less effort as a direct x-ray recorder than as the medium for writing and manufacturing the zone-plate lens that is needed to generate a reference point source for Fourier holography.

2.4 Definition of parameters for in-line holography

Consider a square hologram of half-width x_0 at distance z from the sample subtending a half angle θ as shown in Figure 1. Like any other optical system, such a hologram has a numerical aperture (N.A.) equal to $\sin\theta$ and a diffraction-limited resolution, δ_t, of $\lambda/(2\,\text{N.A.})$, where we assume coherent illumination and λ is the x-ray wavelength. When the sample is small compared to the hologram, the highest fringe frequencies will evidently be recorded at the edge of the hologram and in Figure 1, the fringe frequency at x_0 is that of the beam from the sample (with spatial frequency $\sin\theta/\lambda$) interfering with a reference beam (of spatial frequency zero). The result is a maximum fringe frequency of approximately $x_0/(\lambda z)$ so that the width of half of one fringe period is $\lambda/(2\,\text{N.A.})$. In order to sample this fringe system without loss of information, we must, according to Shannon, sample at twice the maximum frequency. The sampling interval Δ_s must be as good as

$$\Delta_s \leq \frac{\lambda z}{2x_0} = \frac{\lambda}{2(\text{N.A.})} = \delta_t. \tag{1}$$

This is roughly equivalent to the well-known rule that the diffraction-limited resolution of a zone plate is equal to the width of its outer zone. The total number of sampling intervals is N where $N = 2x_0/\Delta_s$. Thus

$$N = \frac{(2x_0)^2}{\lambda z} = \frac{4(\text{N.A.})^2 z}{\lambda} = \frac{\lambda z}{\Delta_s^2}, \tag{2}$$

which is $4\times$ the number of Fresnel zones. This gives us the size ($N \times N$) of the dataset we will have to process.

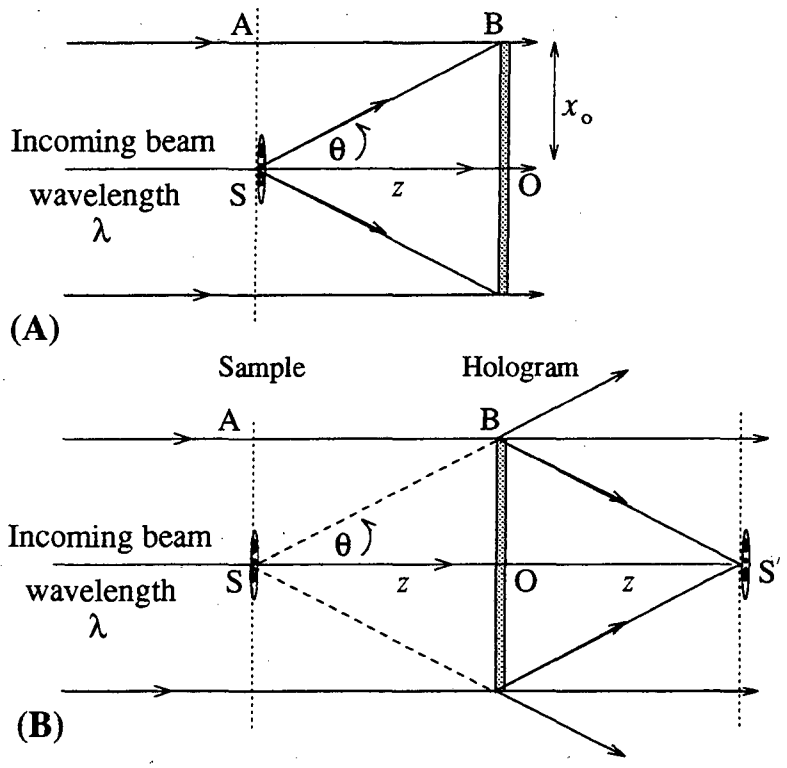

Figure 1: Schematic showing parameters used in our discussion on Gabor holography. The top schematic **(A)** illustrates the recording parameters while the bottom diagram **(B)** shows the reconstruction parameters.

We should recognize that Figure 1 and the above equations are oversimplifications in the sense that we are not really free to choose the size of the hologram arbitrarily. The largest useful value of x_0 (and hence of N.A.) is the value at which the fringes just cease to be discernible because of insufficient detector resolution, signal-to-noise ratio, or x-ray beam coherence.

3 Requirements for an In-line Experiment

In order to mount a successful in-line holography experiment, a number of requirements must be satisfied which we describe in this section. Let us assume that we wish to make holographic images with transverse resolution δ_t using x-rays of prescribed wavelength λ. By Equation 1, Δ_s and N.A. are immediately determined. However x_0 and N are not determined until we choose a value for the working distance z.

3.1 Choice of working distance

The working distance z is almost the only parameter we are free to choose in an in-line holography experiment and in one sense we would like it to be as large as possible. At a given δ_t and N.A., this would lead to a large hologram which would make it easier to satisfy the general transparency requirement of in-line holography and would also lead to a more tractable twin-image-suppression problem. However, increasing z also requires greater monochromaticity and spatial coherence (Equations 3 and 4). In addition, a larger z leads, according to Equation 2, to a larger N for which there are practical computational limits. The reasoning should therefore be to choose the largest N value allowed by coherent x-ray power and available computer hardware. The value of x_0 then follows from Equation 1 and z follows from Equation 2. The monochromaticity and spatial coherence requirements are discussed in the next section.

3.2 Source

Historically, finding a sufficiently powerful source of coherent soft x-rays has been the major challenge. The spatial and temporal coherence requirements can be determined from Figure 1. The coherence length $\lambda^2/\Delta\lambda$ must be greater than the greatest path difference between interfering beams which, from the figure, is $\mathrm{SB} - \mathrm{AB} \simeq x_0^2/2z$. The monochromaticity requirement is thus

$$\frac{\lambda}{\Delta\lambda} > \frac{x_0^2}{2\lambda z} = \frac{(\mathrm{N.A.})^2 z}{2\lambda} = \frac{N}{8} \tag{3}$$

From Figure 1 it is also evident that the greatest transverse separation of incoming rays that will later have to interfere is $\mathrm{AS} = x_0$ so the coherence width (w_c) must be

$$w_c > x_0 = (\mathrm{N.A.})\, z \tag{4}$$

Using a monochromator and suitable apertures we can meet these requirements using almost any soft x-ray source. However, the flux remaining will only be sufficient to record a hologram in a timely fashion if the source has high brightness (flux per unit phase space volume). Undulators currently provide soft x-rays with the highest average brightness and are therefore the most suitable for x-ray holography.

The size of the aperture needed to produce a given coherence width at a prescribed distance is traditionally calculated using the van Cittert-Zernike theorem [Born 1980] which applies to incoherent sources. However, given the strongly directional character of undulator radiation one might suppose that an undulator source must be at least partially coherent. The situation has been investigated by Howells and Kincaid [Howells 1994] who find that in the regime of interest (small sources at great distances), the van Cittert-Zernike theorem results can still be safely used.

According to this theorem, the degree of coherence between the fields at two points in the far field depends only on the distance between the points and not on their absolute positions. Thus, if the source is multimode and unfocused, the illuminated area may be much greater than the coherence width and Gabor holograms of maximum width $2w_c$ can be made anywhere within that area. In fact, by using the whole beam footprint ($\approx 1\,\mathrm{mm}^2$) from the multimode undulator source, we can record many holograms simultaneously.

3.3 Detector

Since the in-line holographic method has no magnifying optics, a high resolution detector is required. According to the arguments in Section 2.4 the detector should be able to record the highest frequency fringes that are present with "sufficient" signal-to-noise ratio. The definition of sufficient signal-to-noise ratio for detection of a fringe system has been discussed by Mueller [Mueller 1976] and by Goodman [Goodman 1985]. To detect the fringe system the detector needs both adequate resolution and detective quantum efficiency (DQE). At present we use a high-resolution photoresist developed for use in electron lithography. We discuss the above quantities in relation to photoresist detectors in Section 4.

3.4 Vacuum

Wet samples naturally have to be illuminated at atmospheric pressure while dried samples can be exposed in-vacuum. However, soft x-rays of $\lambda = 1$ to 5 nm have a $1/e$ attenuation length in air on the order of a millimeter. Thus to conserve photons, x-ray beam transport also requires at least rough vacuum. Operating at ($\sim 10^{-3}$ Torr) is our normal practice which is more than sufficient for x-ray transport. However, our future plans to image frozen-hydrated samples will require 10^{-8} Torr so as to avoid condensation on the specimen. Whatever vacuum is used, the experimental chamber must be separated from the beam-line ultra-high vacuum (UHV) system by an x-ray transparent window for which purpose we use $\sim 100\,\mu$m of silicon nitride (Si_3N_4).

3.5 Readout method

After recording and development the hologram exists as a relief pattern in the surface of the photoresist recording medium. Hence, we must employ a high-resolution examination technique that is sensitive to surface topography. The atomic force microscope (AFM) is the ideal tool since it measures relief directly in contrast to the transmission electron microscope (TEM) which is mainly sensitive to thickness. The AFM allows a hologram to be recorded on a rigid substrate (rather than a thin membrane) and has the additional benefits of requiring no surface preparation, of being non-destructive, and of providing direct digitization of the scanned image. The absence of any

need for metallization is particularly important because it allows one to search for the optimum development by proceeding in steps with AFM monitoring at each step.

We noted above that the hologram must be digitized with a pixel size (Δ_s) no larger than the desired image resolution δ_t. Numerical calculations of the optical performance of Fresnel zone plates (which are a type of hologram) have shown that zones must be correctly placed to an accuracy of about 1/3 of the finest zone width [Simpson 1983, Michette 1986]. Thus, the position of hologram digitization points must be accurate to $\Delta_s/3$. This placement requirement must be met over the entire hologram width $2x_0$, leading to a requirement that the fractional placement error be less than $\Delta_s/(6x_0) = 1/(3N)$. For example to achieve 20 nm resolution at a 500 μm working distance with $\lambda = 2$ nm we would have $N = 2500$ which imposes a requirement for field linearity of about 1 part in 10^4. Such linearity requirements were the main motivation for designing our own custom AFM (described in Section 5).

3.6 Reconstruction method

To achieve sub-50 nm image resolution in x-ray holography, we must record fringes of period 100 nm or smaller. To reconstruct such a hologram optically one cannot use visible light optics to form the final image. However, by treating the resist recording as a reflection phase hologram one can still achieve a reconstruction using UV light [Joyeux 1989b, Joyeux 1988b]. This method offers a rapid and convenient route to the final image but the wavelength of the UV light places limits on the ultimate achievable resolution. Because our first priority is high resolution, we have chosen to seek a numerical representation of the hologram for computer reconstruction of the image. This is equivalent to an optical reconstruction with the original reference wave and is thus aberration-free [Goodman 1967] and visualizable at any required magnification. In addition, computer reconstruction allows the simultaneous determination of both the absorptive and phase shifting properties the reconstructed object.

4 Photoresist recording

The holograms reported here were recorded using the photoresist poly(methyl methacrylate) or PMMA as the detector. PMMA is the highest-resolution organic material commonly used as a photoresist and is suitable for UV, electron and x-ray lithography. Using electron-beam lithography, 10 nm isolated lines have been recorded in PMMA [Ochiai 1991] suggesting that similar resolution can be achieved using soft x-rays. In addition, PMMA is thought to have an x-ray DQE of about 10% [Spiller 1976] although there maybe possibilities for improvement.

PMMA is composed of long-chain molecules. When ionizing radiation (> 4.3 eV) is absorbed, bonds are broken along the main chain as well as between the main chain and side groups. These reactions lower the local molecular weight and thus increase the dissolution rate in a solvent. However, if the exposure is continued to high enough dose levels, cross linking begins to dominate, increasing the local molecular weight and hence reducing the dissolution rate. We have begun to characterize the sensitivity of PMMA as an x-ray detector [Zhang 1995] with the aim of determining optimum exposure/development levels.

After development, a surface relief map is produced with valleys corresponding to high exposure and mountains to low exposure. However, the amount of resist removed is not a linear function

of the x-ray exposure. The dependence of the depth, t_d, of resist removed by the developer as a function of absorbed dose D is well approximated by

$$t_d = T\eta R_0 \left(\frac{D}{D_0}\right)^{\gamma} = kD^{\gamma}, \tag{5}$$

where T is the development time, η is the developer concentration, R_0 has a value in the range $10 - 100\,\mathrm{nm/sec}$ for typical conditions with $D_0 = 10^4$ Gray, and $\gamma \simeq 2$ [Hawryluk 1975]. We will use this relationship with a constant k in an attempt to linearize the x-ray recording during data reduction (section 7.7).

5 Atomic Force Microscope

5.1 Principle of operation

An AFM operates by raster scanning a fine tip across the sample surface. The tip is attached to the end of a miniature cantilever which has a suitably small spring constant (Figure 4). Near a surface, the major forces acting on the tip are the van der Waals force between the tip and the surface, and the spring force of the cantilever. The operation of an AFM can be based either on the very short range repulsive van der Waals force (contact mode) or on the longer range, but weaker, attractive force (non-contact mode) [Sarid 1991]. We have used contact mode exclusively and, in spite of the softness of the polymer surfaces we have been examining, we have not seen evidence of probe damage to the surface. This observation is in agreement with the experience of practitioners of x-ray contact microscopy who also use an AFM in contact mode to scan PMMA surfaces [Stead 1992, Stead 1995].

The microscope operates by detecting the displacement of the lever due to the atomic force and then applying a feedback-controlled displacement of the sample to maintain a constant cantilever deflection (*i.e.* constant force) as the scan proceeds.

There are many methods to determine the cantilever deflection. The most ubiquitous, and the one we use, is an optical lever. Light from a laser is reflected off the cantilever's back surface into a split photodiode. Bending the cantilever moves some light from one half of the photodiode to the other. The difference of the photodiode currents is then used to provide the feedback signal to the sample driver (Figure 4) which moves the sample so as to null the difference signal.

Most commercial AFMs use piezoelectric translators to provide the scan motion. Calibration curves of the scan field are then used to reduce non-linearities to a level acceptable for most applications. These calibration curves are either used in software to correct (undistort) images or are used to adjust the piezo voltage to obtain undistorted images. In either case the images still suffer from distortions far greater than the tolerance for high-resolution holography (see Section 3.5). This is because as it is difficult to accurately calibrate piezoelectric devices since their position is a function of scan speed, past position, humidity and temperature as well as applied voltage. In one commercial AFM system with optical position feedback we still measured $\sim 1\%$ field nonlinearities. These linearity problems are overcome in our AFM system by using capacitance micrometers to accurately index the x-y scan motion via a closed-loop feedback system [Griffith 1994, Browne 1992] as described in the next section.

5.2 Flexured x-y scanning stage

We have used a monolithic design with flexural hinges to implement a combined x-y motion stage to scan the sample in x and y while the tip is held fixed. Figure 2 shows one bending element from the stage. It is constructed from two cantilevers each of length $l/2$ joined by a rigid center piece of

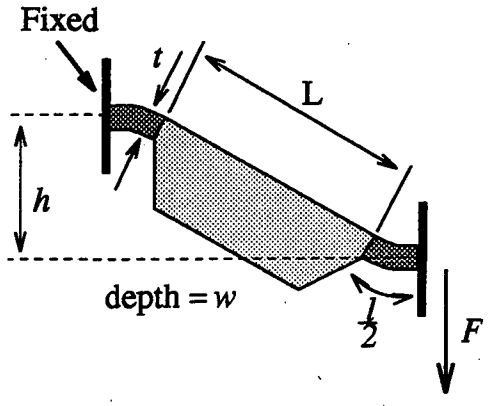

Figure 2: Schematic of one bending element from out stage. When used in the whole stage the hinge is designed to translate along F without rotation. Table 1 lists the hinge dimensions.

length L. For this element the displacement h due to a force F is

$$h = \frac{l^2}{4EI}(\frac{l}{3} + \frac{L}{2})F, \tag{6}$$

where E is Young's modulus and I is the section moment of inertia. For a beam of rectangular cross-section $I = wt^3/(12)$, where w is the width and t is the thickness of the beam. This allows the spring constant, $k = |F/h|$, to be easily calculated.

Each linear stage axis is composed of four pairs of these elements, as shown in Figure 3, which represents two classical rectilinear motion mechanisms [Becker 1987, Smith 1992], one inside the other. By this design we are able to achieve extremely good orthogonality and independence of the x and y drives. Since the stage is not compact, its thermal expansion during a scan must be considered. We discuss this further below.

The design parameters for our custom aluminum stage are given in Table 1. Using these values in Equation 6 we calculate an effective spring constant of 5.5×10^5 N/m which is in good agreement with the measured value of $(6.0 \pm 0.5) \times 10^5$ N/m. Using an accelerometer we measured a resonant frequency of 150 Hz for the inner (x) axis which is safely above our piezo's maximum slew rate of 20 Hz and in good agreement with the value of 140 Hz calculated from the above value of the spring constant and the estimated mass of the moving part of the stage.

In order to attain good absolute positioning accuracy we used Queensgate Instrument piezo drive systems with built-in indexing [Queensgate]. The system generates an indexing signal derived from a capacitive sensor consisting of two parallel plates whose separation is determined by measuring their capacitance with an A.C. bridge. The Queensgate devices we use have a departure from linearity of about 4 parts in 10^4 over a 75 μm range. However, the linearity curve is stable and reproducible and can be utilized to achieve absolute positioning accuracy of $\sim$ 1 nm or just over 1 part in 10^4. The electronic readout noise is $0.005\,\text{nm}/\sqrt{\text{Hz}}$, *i.e.* 0.5 nm at our present maximum scanning frequency of 10 kHz.

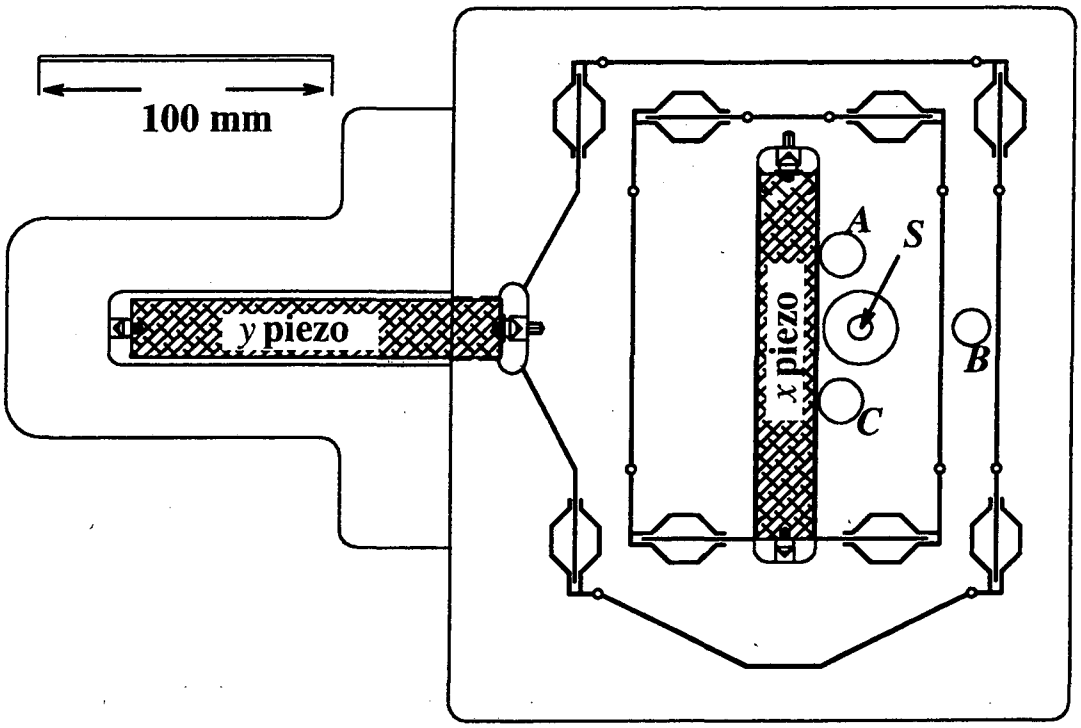

Figure 3: The custom stage built for the atomic force microscope. The inner stage is the fast (x) axis. The two piezos are oriented orthogonal to one another. A, B and C are through holes for the tripod-mounted cantilever deflection sensing unit, while S is the mounting hole for the z-piezo.

t	(thickness)	1.42 mm
w	(depth)	28.7 mm
L		22.25 mm
l		5.7 mm

Table 1: Design values for the aluminum stage's flexure dimensions. Refer to Figure 2 for a schematic of the hinge.

5.3 AFM system architecture and control

Our stage scans the sample in x and y below a fixed tip mounted in a commercial AFM cantilever-deflection sensing unit which we have interfaced to our computer. The system used to control the AFM is shown in Figure 4. The sample is mounted on the scanning stage via another piezo (the z piezo depicted in Figure 4) which drives it toward or away from the tip.

There are three principal elements to control; 1) the raster scan (x and y axes), 2) the sample's position relative to the tip (via the z-piezo), and 3) the data acquisition. To control the x and y

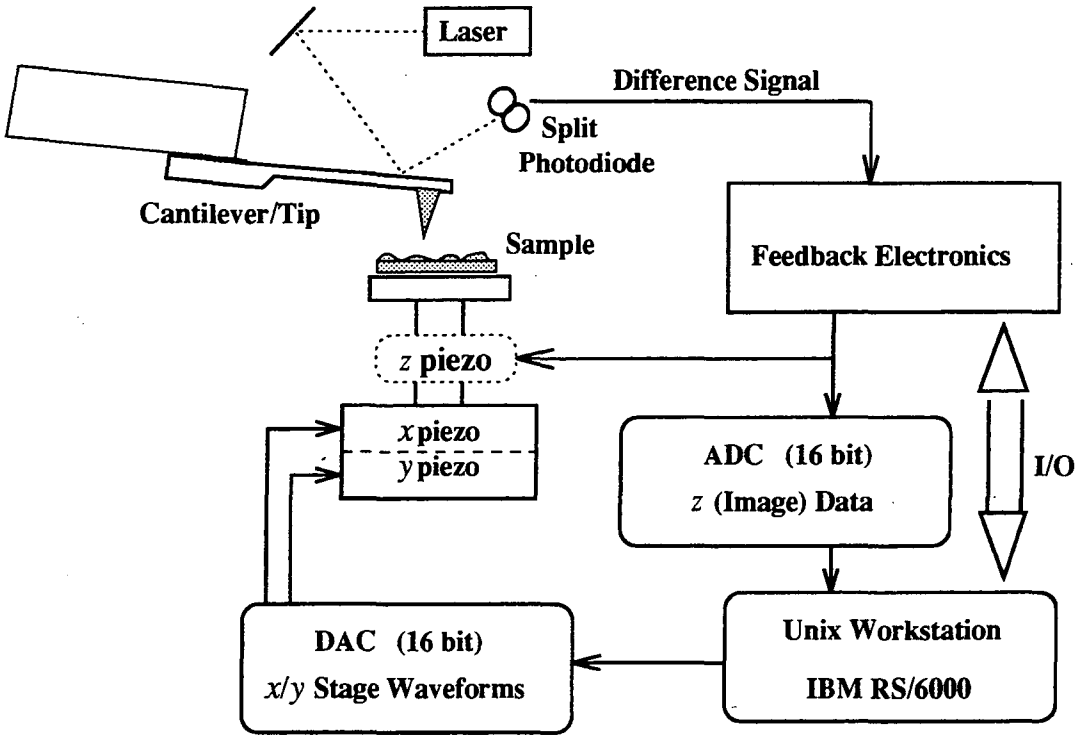

Figure 4: Schematic of our custom atomic force microscope's interface. Forces acting on the probe tip cause the cantilever to bend which is monitored by a sensor. The signal is then used in the z-drive feedback which regulates the sample-tip force.

scans we use a 16-bit digital-to-analog converter (DAC) with two output channels programmed to produce staircase functions. We require the 16-bit accuracy to take full advantage of the Queensgate piezo's indexing resolution ($\sim 1\,\text{nm}$) and range ($\sim 75\,\mu\text{m}$).

The commercial cantilever-deflection sensing unit delivers the amplified sum and difference signals from the split photodiode. The integral of the difference signal is used to generate the z-piezo voltage and is also the signal used to record the surface height at each pixel.

A 16-bit analog-to-digital converter (ADC) (with eight input channels) is used to collect the value of the feedback controlled z-piezo drive voltage for each pixel as well as environmental data (air and stage temperatures along with humidity) after each scanned row. Both the DAC and the ADC have sufficient internal memory so that the computer is only involved at the beginning and end of a scan line.

Interfaces were constructed to both the commercial deflection sensing head and the Queensgate piezo drivers. The hardware is controlled via an IEEE 488.2 interface to an IBM RS/6000 UNIX

workstation. By using a UNIX workstation to control our system we are able to acquire virtually any size dataset (a flexibility commercial AFMs do not have). In addition the extra computational power and memory management capabilities of our IBM RISC machine are highly advantageous when reconstructing holograms (a single 2048×2048 complex floating point array occupies 64 Mbytes of computer memory).

5.4 Sample alignment

We use two optical microscopes to align the tip and the sample. An optical microscope with a long-working-distance toolmaker's objective is used to view the hologram from above and position the tip over the region of interest. A stereo microscope views the sample and tip from the side and is used when the tip is approaching the sample to monitor the tip-to-sample distance so as to avoid plowing into the surface.

5.5 AFM environment

To achieve atomic resolution, most atomic force microscopes are designed to be light and stiff, giving them high resonant frequencies and therefore good isolation from vibrational noise. Our AFM has less need of such isolation since atomic resolution imaging is not a goal of the present work (nor a possibility given the $\sim 0.005\,\mathrm{nm}/\sqrt{\mathrm{Hz}}$ position noise of the capacitance micrometers). Instead, our requirement is to meet the field linearity requirements outlined in Section 3.5 over an AFM scan time which can be as long as 30 minutes (e.g., 2048×2048 pixels scanned unidirectionally with a 0.1 msec pixel dwell time). In order to minimize drifts which would misplace pixels from their theoretical positions and therefore lead to hologram and finally image aberrations, a large thermal mass is favored. Given mechanical paths of about 20 cm between the AFM head and the sample scan mechanism, the temperature of the flexure stage should remain constant to about 0.1° C during a scan with the aluminum flexure stage now used. (Thermal stability could be gained by making the flexure stage out of Invar, although the lower coefficient of thermal expansion of invar is partly offset by its low thermal diffusivity which leads to a slow approach to thermal equilibrium following a change in heat input). We use an insulated enclosure to provide acoustic, thermal and optical isolation of the AFM during operation, and abandon the scan if a stage-mounted thermocouple indicates temperature changes which exceed our limits. The AFM is also mounted on an air table and rests on a stack of steel plates with viton spacers for vibration damping.

5.6 Demonstrated performance tests

We have imaged gratings which were well characterized independently and have so far demonstrated that the scan linearity of our AFM is 0.05% or better. We believe we will be able to demonstrate the expected value of 0.01% when we have implemented an indexed type of z piezo. The best measure of performance is the reconstructed image quality from actual holograms. Figure 5 is a Fresnel hologram of a gold wire ($12\,\mu$m in diameter) with a lineplot taken from the indicated region. The fringes that can be seen at the edge of the scanned hologram and the successful reconstruction of the holograms to give high-quality images lead us to believe the stage is operating as designed.

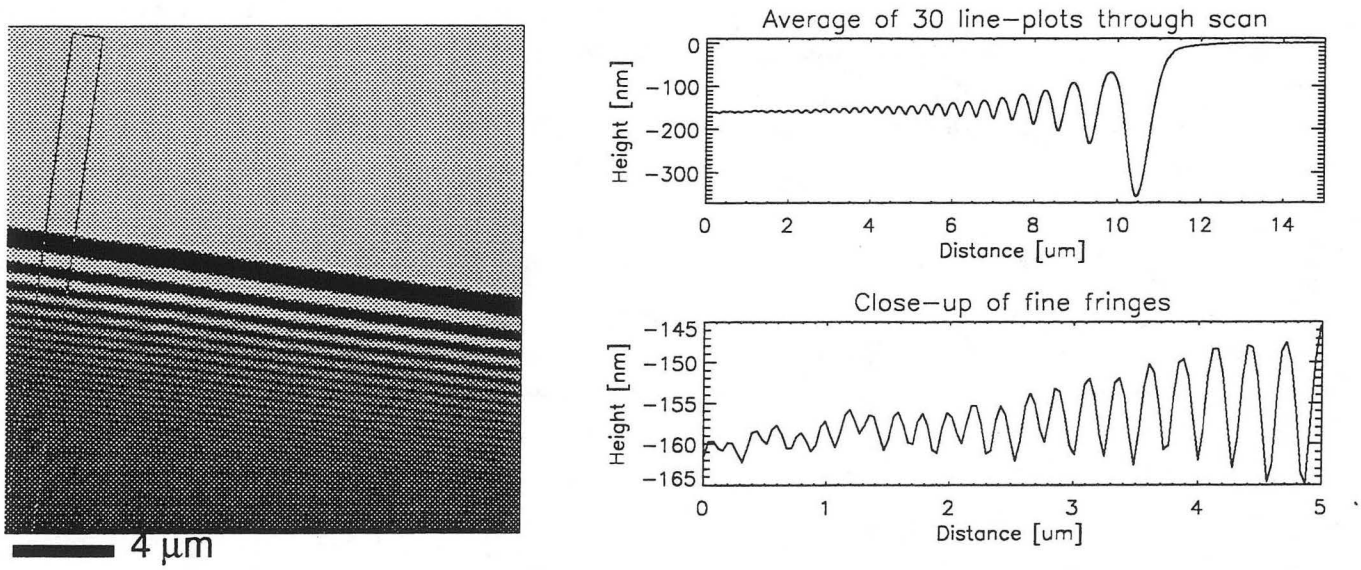

Figure 5: Gabor hologram from a 12 μm diameter gold wire. The plots show the average of the 30 lines outlined in the image. Fringes are visible out to the edge of the field of view. The plots show a fringe positioning accuracy of < 0.1 μm and a height resolution of about 1 nm.

6 Numerical Reconstruction

6.1 Theory

The holograms are recorded using plane waves in the in-line geometry with a specimen-to-hologram working distance of z. In principle, we could reconstruct the hologram by placing it in the original illuminating wave and observing the real image a distance z downstream. To mimic this numerically we have to modulate a plane wave by the recorded hologram function, and numerically propagate it by a distance z to calculate the intensity distribution at the real-image plane. This produces the same result we would get in the equivalent laboratory process: the true image plus a second hologram of the sample at the distance $2z$ (see Section 2.1).

We propagate the plane wave $\psi_0(x, y:0)$ modulated by the function $g(x, y)$ to the image plane (i) by

$$\psi(x_i, y_i : z) = \iint_{-\infty}^{\infty} \psi_0(x, y : 0) g(x, y)\; h(x_i - x, y_i - y : z)\, dx\, dy. \tag{7}$$

The propagator function $h()$ is given in the Rayleigh-Sommerfeld formulation [Goodman 1968] as

$$h(x_i - x, y_i - y : z) = \frac{i}{\lambda} \frac{\exp[-i2\pi r/\lambda]}{r} \cos\theta, \tag{8}$$

where $r^2 = (x_i - x)^2 + (y_i - y)^2 + z^2$ and r is the distance from a point in the hologram plane to a point in the image plane, θ is the angle between the direction of r and the axis, and $\cos\theta = z/r$ is the obliquity factor. Applying the convolution theorem we can express Equation 7 as

$$\psi(x_i, y_i : z) = \mathcal{F}^{-1}\Big\{ G(f_x, f_y) \cdot H(f_x, f_y : z) \Big\}, \tag{9}$$

where we use $\mathcal{F}$ to represent a Fourier transform so that $G(f_x, f_y) = \mathcal{F}\{g(x,y)\}$ *etc.* and f_x is the spatial frequency corresponding to x. The propagator function can be expressed exactly in transform space [Collier 1971, Appendix 1] as

$$\begin{aligned} H(f_x, f_y : z) &= \exp[-i2\pi\frac{z}{\lambda}(1 - f_x^2 - f_y^2)^{1/2}], \\ &= \exp[-i2\pi\frac{z}{\lambda}]\exp\left[i\pi\lambda z(f_x^2 + f_y^2) + \frac{i\pi\lambda^3 z}{4}(f_x^2 + f_y^2)^2 + \ldots\right]. \end{aligned} \tag{10}$$

Ignoring the constant phase factor and using the Fresnel approximation we can write

$$H(f_x, f_y : z) \simeq \exp[i\pi\lambda z(f_x^2 + f_y^2)]. \tag{11}$$

This approximation is usually valid in the regime in which we operate; however, the additional terms shown in Equation 10 are used in our reconstruction algorithm if their effect is significant.

6.2 Twin-image problem

The origin of the twin-image artifact was explained in Section 2.1. The conventional approach to eliminating it is to use iterative "phase-retrieval" algorithms such as those developed by Gerchberg and Saxton [Gerchberg 1972] and Fienup [Fienup 1980]. Applications of this type of algorithm to x-ray holography have been reported in a preliminary way by us [Jacobsen 1992a] and by Koren and coworkers [Koren 1993]. The algorithms work by propagating a complex wave field back and forth between the object and hologram planes. At each plane constraints are applied: at the hologram the intensities are constrained to equal the measured ones. At the object plane, the constraint might be that the empty parts of the field of view are forced to have a transparency of unity (the "finite-support" constraint). The intention is that the procedure should converge toward a unique object transparency function which satisfies the object-plane constraints and which diffracts an incoming plane wave into the measured hologram. We have implemented an algorithm consisting of combinations of the algorithms of Gerchberg and Saxton and of Fienup. The simplest form of this approach, where only the finite-support constraint is applied at the object plane, has been very successful in removing the twin-image signal when the object is small and well isolated. It is less successful in cases where there are many strong scatterers inside or just outside the hologram area. This is a complex problem and is the subject of continuing research on which we will report more fully in the future. We believe that the problem will yield to further efforts in all cases where the sample is sufficiently sparse for in-line holography to work at all.

6.3 Effect of z-piezo errors

While our custom AFM has excellent x-y scan linearity, the z-piezo is presently a conventional piezoelectric translator operating without feedback or calibration. Such devices have inherent hysteresis and other errors so that our height measurements (hologram intensities) presently have an absolute distortion of 10–20%. This is not as important as it might seem since, to first order, errors in reading the resist height are equivalent to photographic film nonlinearities which are known to have only a modest effect on reconstructed hologram image quality [Collier 1971]. This is related to the fact that recovery of a complex wavefield from its phase (fringe position) is much easier than from its amplitude (fringe height) [Stark 1987, Chapter 8]. Nonetheless, we are working toward reducing these errors by fitting a capacitive sensor to the z-piezo.

7 Our Experiment

One of the desirable features of x-ray holographic microscopy is the simplicity of the part of the experiment that involves the sample and x-ray beam (see Figure 7). The specimen does not need to be accurately aligned relative to anything except the beam which is about 1 mm^2 in area. While the distance from the specimen to the photoresist must remain accurately constant during the hologram exposure, the actual value used is not crucial (it can be determined during the numerical reconstruction). This is the property that makes the Gabor geometry well suited to experiments with flash x-ray sources such as x-ray lasers [Trebes 1987, Trebes 1992].

7.1 NSLS beamline X1A

Soft x-ray undulators at synchrotron radiation centers currently provide sufficient coherent power to enable Gabor holograms to be easily recorded. For the work reported here we used the 8-cm-period undulator at the X1A beamline[Rarback 1990, Jacobsen 1994] at the National Synchrotron Light Source at Brookhaven National Laboratory which has a brightness more than ten orders of magnitude higher than a typical microfocus x-ray tube. Figure 6 is a schematic of the optical layout of the X1A beamline. In 1996 we plan to continue our experimental program on an even brighter undulator source at the Advanced Light Source at the Lawrence Berkeley National Laboratory.

7.2 Effective source: wavelength, coherence, flux

While wet biological specimens are best studied using "water window" soft x-rays with $2.3\,\text{nm} < \lambda < 4.4\,\text{nm}$; the studies reported here are on dry specimens, so the experimentally convenient wavelength of $\lambda = 1.89\,\text{nm}$ was used. For a typical sample-hologram spacing of $\sim 500\,\mu\text{m}$ and using Equations 1 and 3, we see that to obtain 40 nm resolution in this case we require spatial coherence over a transverse distance $x_0 \gtrsim 15\,\mu\text{m}$ and $\lambda/\Delta\lambda \gtrsim 80$. In the actual experiment we used a $40\,\mu\text{m}$ exit slit (with a $100\,\mu\text{m}$ entrance slit) so that we had $\lambda/\Delta\lambda > 400$, a horizontal coherence width of $50\,\mu\text{m}$ and a vertical coherence width $\gtrsim 200\,\mu\text{m}$. The flux delivered to the sample for in-vacuum experiments was $\sim 10^5$ photons/sec/$(\mu\text{m})^2$ per 100 mA of stored electrons in the synchrotron storage ring. We could have chosen to concentrate the beam into a smaller area with optics but this would not have made the exposure time short enough to avoid radiation damage while it would have made targeting more difficult and risked complications due to imperfect optics.

7.3 PMMA

We used a solution of 9% by weight PMMA (molecular weight = 9.7×10^5 Daltons) in cholorobenzene spun at 4.5 krpm onto glass substrates resulting in $\sim 1\,\mu\text{m}$ films. The photoresist film was baked at 150° for two hours. The bake serves to outgas adsorbed gases and maximizes PMMA chain scission relative to crosslinking upon irradiation [Zhang 1995]. The glass substrates were cut from microscope slides and cleaned in preparation for spinning. We found that high relative humidity ($> 50\%$) frustrated the PMMA film's adhesion to the glass substrate.

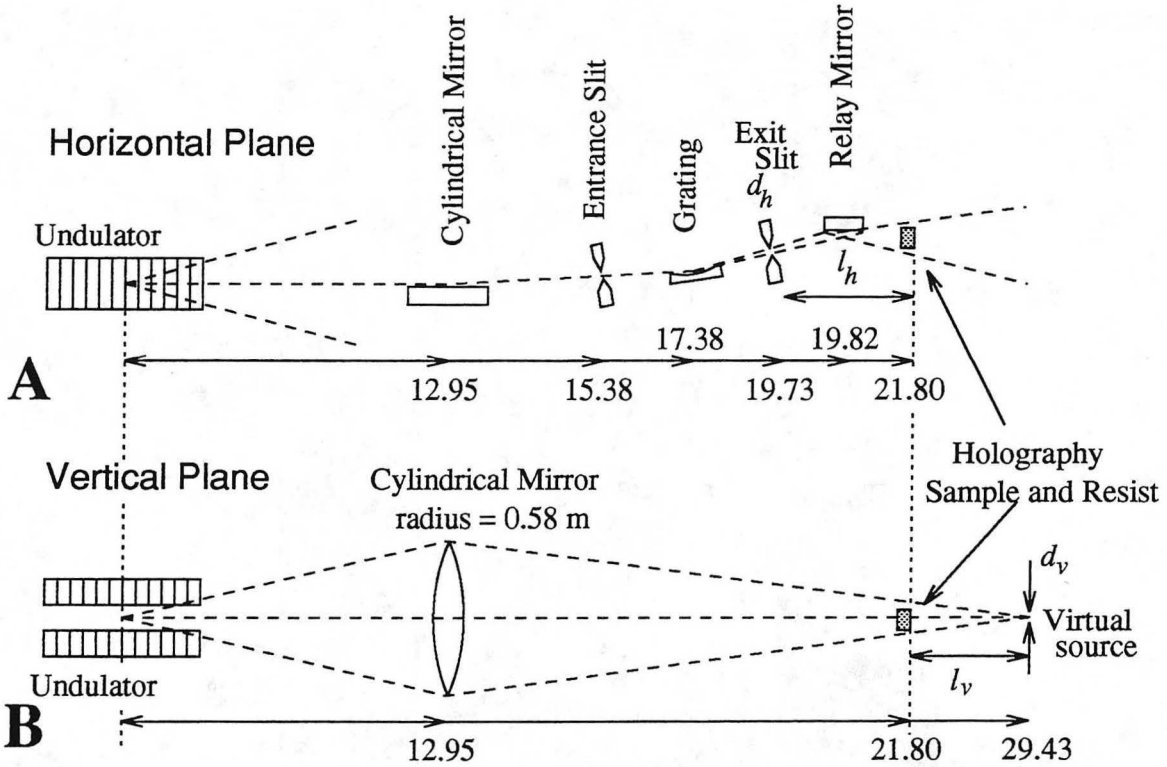

Figure 6: Optical layout of the X-1A beamline at the National Synchrotron Light Source. The numbers correspond to the distance in meters from the optical element to the undulator center which has a horizontal source size 390 μm and a vertical source size 18 μm (both rms half widths). In the horizontal plane (**A**), the exit slit (width d_h) of a spherical grating monochromator is used as a spatial filter for coherent illumination of the hologram located a distance $l_h = 1.98$ m away from it. In the vertical plane (**B**), a cylindrical mirror produces a vertical source of height $d_v = 23\,\mu$m at a distance $l_v = 7.63$ m *downstream* of the sample.

7.4 Atomic force microscope

The atomic force microscope delivers a digital map of developed resist thickness measured with a pixel size Δ_s over a field $(2x_0)^2$. Since we use fast Fourier transforms it is advantageous to set the array size to be a power of 2 (*i.e.* 1024×1024) and adjust the pixel size accordingly. Thus, for $N = 1024$, $\lambda = 1.89$ nm and $z \simeq 500\,\mu$m we use $\Delta_s \simeq 32$ nm and $2x_0 = 33\,\mu$m. From Equation 1 this leads to a potential resolution of 40 nm.

We used AFM cantilevers with a spring constant of $k < 0.01$ N/m so the force exerted on the sample by the tip was typically less than 10^{-9} N. This force was sufficiently weak that the boundaries of the scan areas could not be seen on subsequent scans leading us to believe that no surface damage occurred.

7.5 Sample mounting

Depending on the sample we either used a Si_3N_4 window or a standard electron microscope grid as a holder. A spacer plate was then used to set an approximate value of the object-to-hologram

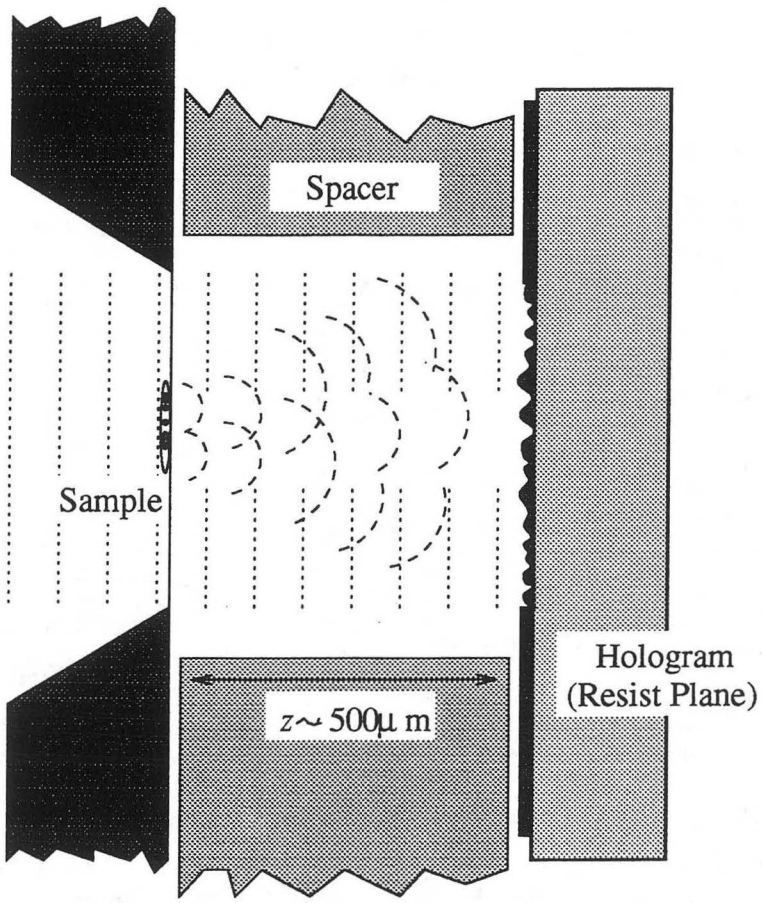

Figure 7: The photoresist used to record the hologram is rigidly mounted to the specimen support using a spacer to set the specimen-to-hologram distance, z.

distance z. The frame of the Si_3N_4 window (or the grid) carrying the objects was then clamped to one side of the spacer and the photoresist substrate to the other side (Figure 7). This ensured a rigid mechanical connection between the object and the holographic recording medium, allowing high-contrast fringes to be obtained without any harmful vibration effects.

7.6 Experimental procedure

The object–hologram packages were aligned to the x-ray beam in a vacuum chamber and the holograms were recorded over exposure times of a half to a few minutes. The exposure time was chosen to deliver $\sim 6 \times 10^7$ photons/$(\mu\text{m})^2$ to the photoresist (10^5 photons/$(40\,\text{nm})^2$ giving 1% shot-noise statistics if the resist DQE is 10%). Photon fluxes were monitored and controlled using a retractable calibrated aluminum photodiode.

We assessed the recorded holograms using an optical microscope with differential interference (or Nomarski) contrast. Good candidates for development were chosen by looking for weak self-development which is a purely qualitative assessment. The photoresist was developed by immersion in a mixture of 1 part methyl isobutyl ketone (MIBK) to 5 parts isopropyl alcohol (IPA) for 5–30 seconds, briefly "rinsed" in isopropyl alcohol, and dried with a filtered jet of nitrogen gas. The first

few (typically 5) Fresnel diffraction fringes ($\gtrsim 500\,\mathrm{nm}$ width, $\sim 200\,\mathrm{nm}$ depth) could be seen in the optical microscope and were used to assess hologram exposure.

Since the AFM examination technique is non-destructive and does not require surface preparation, further liquid development is always possible. This has allowed us to become more conservative in our development of potentially good exposures.

7.7 Data reduction and image reconstruction

Since PMMA is not a linear recording medium, we must find a mapping from measured resist thickness to the recorded hologram irradiance $I(x,y)$. Equation 5 indicates that the remaining thickness of developed resist $t(x,y)$ can be written in the form

$$t(x,y) = t_0 - k\Big[I(x,y)\Big]^{\gamma}, \tag{12}$$

where $\gamma \simeq 2$ for PMMA and k is a constant. We can therefore write $I(x,y)$ as

$$I(x,y) = \Big(\frac{t_0 - t(x,y)}{k}\Big)^{1/\gamma}. \tag{13}$$

In an AFM readout which includes unexposed areas such as the shadows of dense objects, we can take t_0 to be the maximum resist thickness. We usually adjust the parameter $(1/k)^{1/\gamma}$ to set $I(x,y)$ around 1 for numerical convenience. In an optical reconstruction with a linear recording medium, a wavefield with uniform phase and an amplitude equal to the square root of the recorded hologram irradiance would be launched from the hologram toward the image plane. Hence, we set the hologram function $g(x,y)$ of Equation 7 to be $\sqrt{I(x,y)}$ with a phase of zero.

To reconstruct the hologram, the wavefield $\psi_0(x,y:0)g(x,y)$ is then propagated a distance z using Equation 9. The propagation involves a Fourier transform operation on $g(x,y)$, an array multiplication with $H(f_x,f_y:z)$, and an inverse Fourier transform operation.

Before carrying out the final calculation a small subregion of this wavefield is extracted and used to form reconstructed images at a variety of values of z about the expected object-to-hologram distance. From the sharpness of these images (using larger subregions as the true z is approached) the best z value is obtained.

8 Results

Although our long-term aim is to use x-ray holography to image thick hydrated samples, the present investigation was carried out with dried samples. One was a diatom which we used, like many others before us, because its step-like features are suitable for assessing the imaging system resolution. To show the capability to image more complex biological objects we chose a dried cell. This cell was thin enough to allow TEM examination for comparative microscopy, and was capable of withstanding the radiation dose needed for hologram recording. Moreover, it still allowed us to demonstrate many of the important aspects of x-ray holographic microscopy as we now practice it.

8.1 Diatom hologram: demonstration of resolution

A Si_3N_4 membrane containing diatoms was mounted in our chamber as described above. We used $\lambda = 2.23\,\text{nm}$ x-rays exposed for 20 seconds delivering $1.5 \times 10^7\,\text{photons}/\mu\text{m}^2$. The photoresist containing the hologram was developed in 1 part MIBK and 5 parts IPA for 30 seconds and then digitized using the AFM with a step size of 31 nm. The hologram was reconstructed at a distance of $z = 460\,\mu\text{m}$ with no twin-image suppression algorithm used.

Figure 8 shows a line scan across the reconstructed image of a part of the diatom resembling a parallel-sided opaque strip. The strong ringing signals on both sides of both edges is due to twin-image noise and appears as predicted by the theoretical calculations which have been done for this type of object [Tyler 1976]. In spite of the harm done to the overall fidelity of the image by the twin-image noise, it is still possible to estimate the system resolution from the sharpness of the step. We make the conservative assumption that the step is ideally sharp and all of the finite width of its image is due to blurring by the imaging system. Taking the 20-80% step height we arrive at a value of $\sim 40\,\text{nm}$ for the resolution.

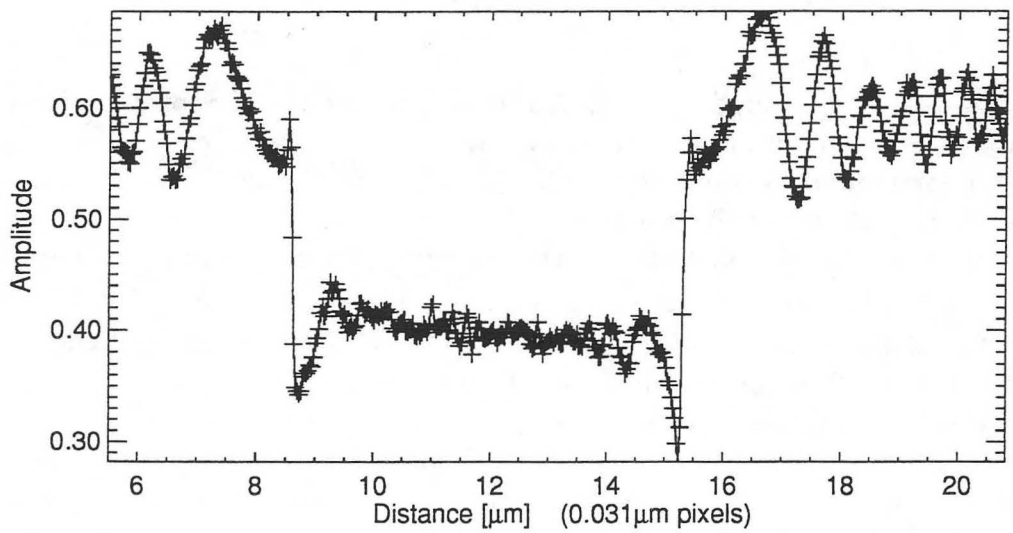

Figure 8: Line trace across the edge of a reconstructed hologram of a diatom with each pixel indicated by a hatch mark. We take as a measure of our resolution the distance it takes to go from 20% to 80% of the maximum amplitude. This distance is 1 or 2 pixels each of which is 31 nm. The ripples are due to twin-image noise and expected from theoretical calculations (see text).

It is of interest to understand what determines this value. The hologram was scanned on an AFM grid spacing of 31 nm, so the resolution is close enough to the expected diffraction limit given by Equation 1 that we cannot rule out the possibility that there is higher-resolution information in the hologram that is lost due to the choice of Δ_s. One way to address this question is to scan a typical hologram area at a much smaller pixel size and examine the power spectrum. Such an examination reveals that the power spectrum of a hologram scanned with $(10\,\text{nm})^2$ pixels roll off to white noise at $\sim 25\,\mu\text{m}^{-1}$ suggesting that information is encoded at the 20 nm resolution level. However, to utilize this information, we would have to scan at both a finer grid and a larger area which would challenge both the power of our computer and the temperature stability of our AFM.

Thus we believe that the resolution of the holograms and reconstructions we have made in this study represent the limitations imposed by our present experimental apparatus and not a fundamental limit of the technique or the resist.

8.2 Holographic microscopy of a dried cell

To demonstrate x-ray holography with a biological sample we used NIL8 hamster neural fibroblasts. These were readily available in our lab, and were grown in culture for 1 to 2 days on a formvar-stabilized carbon film that had been deposited on a gold electron microscope grid (copper grids are not compatible with cell culture). The individual cells adhered well to the grid and spread out so that they were typically 1 to 2 microns thick when wet. To prepare the cells for imaging they were glutaraldehyde fixed and critical point dried.

A grid containing the cells was mounted in our chamber as described above. We used $\lambda = 1.89\,\mathrm{nm}$ x-rays and delivered an estimated dose of 75×10^4 Gray to the sample. The photoresist containing the hologram was developed in a solution of 1 part MIBK to 5 parts IPA for 10 seconds and digitized using the AFM with a step size of 31 nm. The hologram was reconstructed at a distance of $z = 415\,\mu\mathrm{m}$ with no twin-image suppression algorithm used.

Following hologram reconstruction, we took correlative pictures of the cell region. A visible light microscope with a 100×, N.A.=0.9 dry lens was used to image the cell in reflected differential interference contrast. The cell was then carbon coated and imaged in a JEOL 1200 transmission electron microscope at an accelerating voltage of 100 keV and magnifications of 2,000–10,000×. The electron microscope delivered high contrast images of thin regions of this *dry* sample; in future experiments on frozen-hydrated specimens with water thicknesses of a few microns, we do not expect to be able to take high contrast correlative micrographs using electron microscopy.

Figure 9 is an overall view of the cell's pseudopod while Figures 10–13 show various subregions at higher magnification.

9 Discussion

The examples shown in Figures 9–13 demonstrate that we can produce holographic images of complex biological samples without use of prior knowledge. The similarity of the holographic images to the transmission electron microscope (TEM) and visible light microscope (VLM) images gives us confidence that the entire x-ray holographic procedure is working correctly. However, the x-ray reconstructions would benefit from twin-image reduction. For example, the ripples parallel to the main stem in the x-ray image in Figure 10 are absent in the other two images and are clearly twin-image noise. Nevertheless, the true sample features (within the resolution limit) are evidently rendered faithfully in the x-ray images. Furthermore, there is a good deal of information that is absent from the visible light microscope images that is successfully resolved in the x-ray ones. In particular, the tendril seen in the x-ray image in Figure 10 cannot be seen in the optical micrograph, while the transmission electron microscope image provides clear confirmation that it is not an artifact. Another region of interest is the central area shown in Figure 12. This is a region of the cell which violates the requirement for high average transparency of the hologram area. However, comparison to the TEM image again shows that the features in the reconstructed

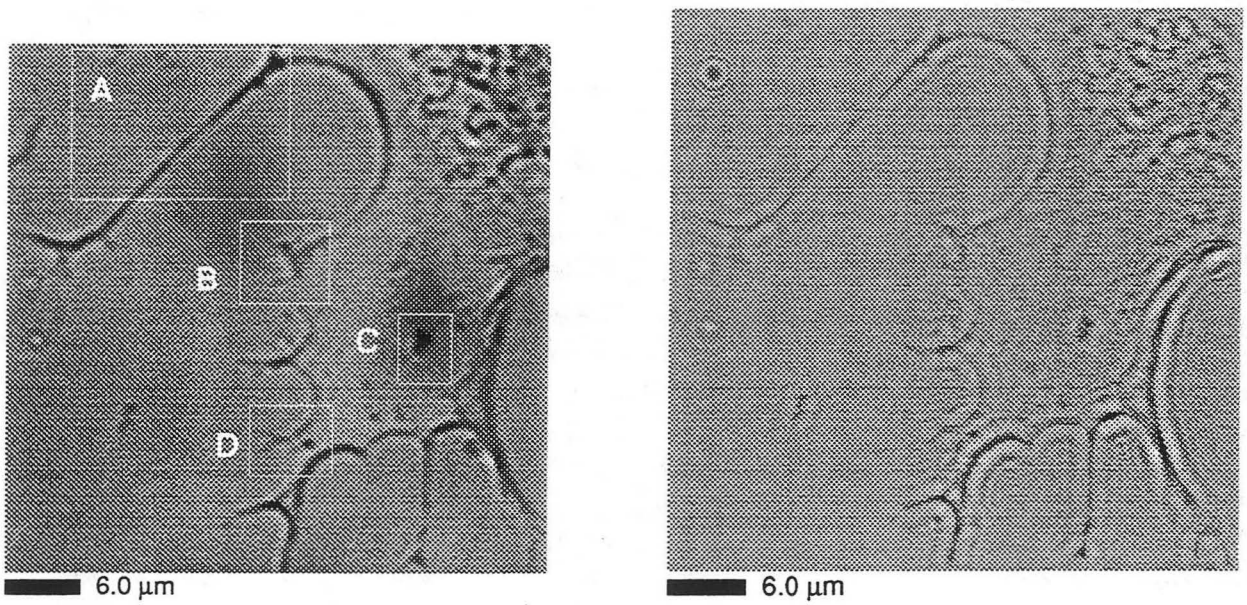

Visible light X-ray

Figure 9: Visible light micrograph (left) and reconstructed x-ray hologram (right) of a critical point dried NIL8 hamster neural fibroblast which was grown in culture on a film supported by a gold mesh. Much of the cell is out of this field of view; the nucleus is beyond the upper right boundary of this image. Many intercellular organelles are shown at the upper right corner, and further structures are shown within the pseudopod at center right in the image. The boxed areas are shown in greater detail in visible light, x-ray holographic, and transmission electron micrographs as follows: **A:** Figure 10, **B:** Figure 11, **C:** Figure 12, and **D:** Figure 13.

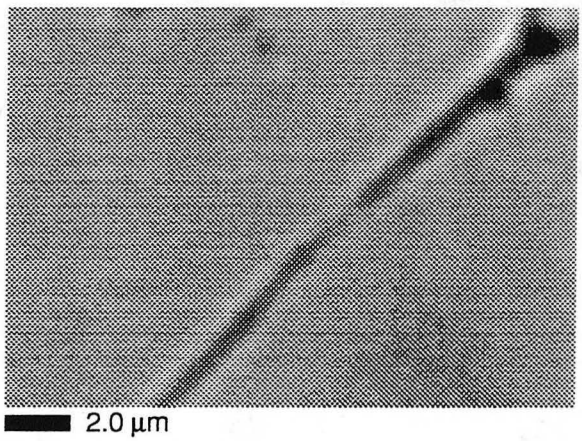

Visible light

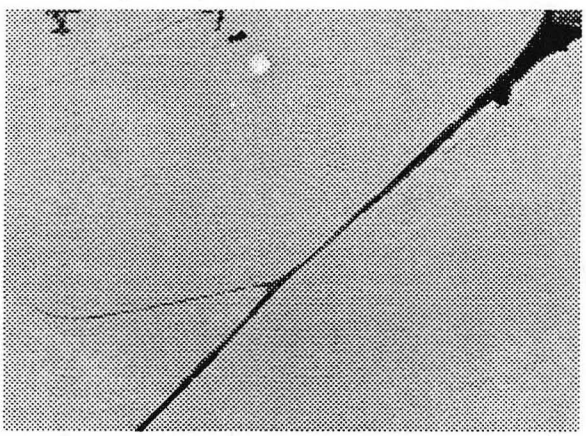

Electron

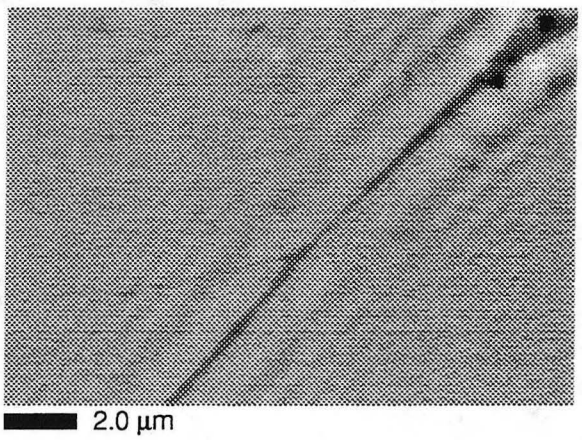

X-ray

Figure 10: Visible light, x-ray holographic, and transmission electron micrographs of a long protrusion from the NIL8 cell shown in region A of Figure 9. The x-ray image shows clearly the organelles at upper right in the image, and the very small tendril at lower left which is difficult to see in the visible light micrograph.

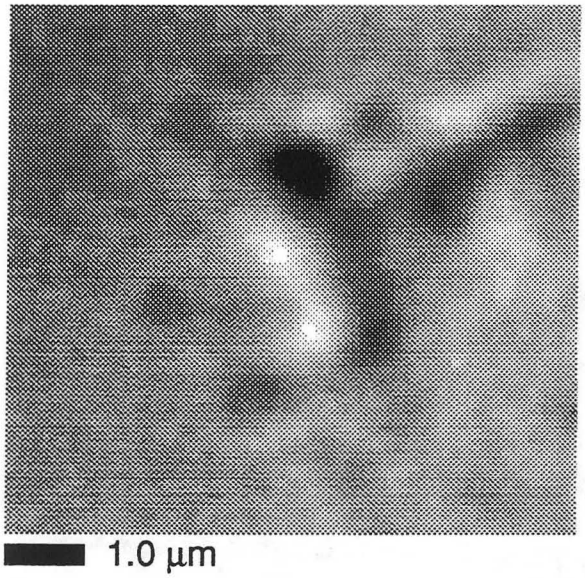

Visible light

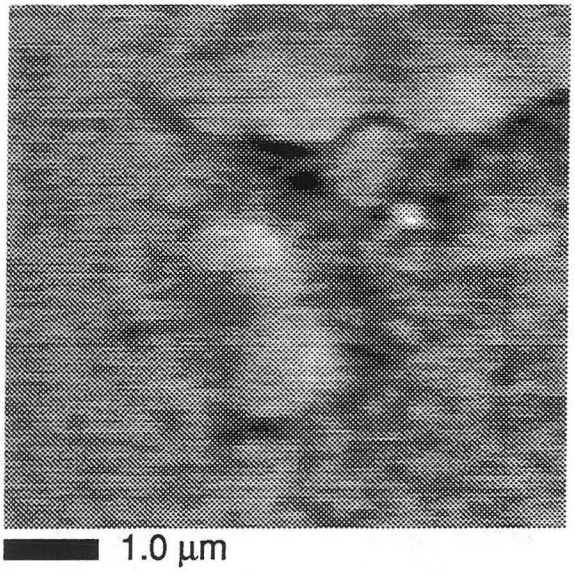

X-ray

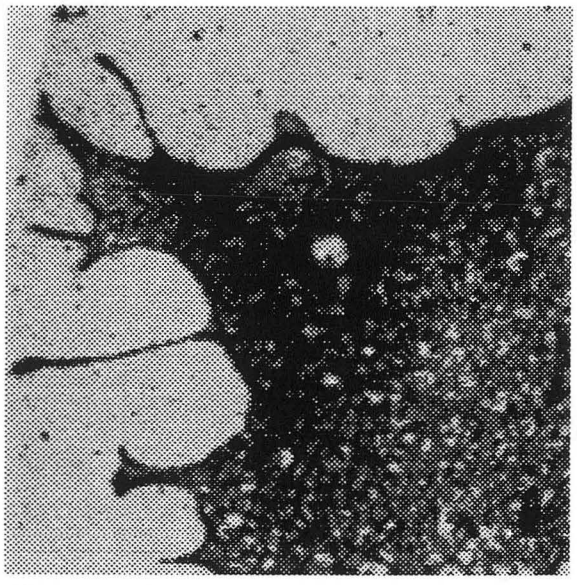

Electron

Figure 11: Visible light, x-ray holographic, and transmission electron micrographs of the edge of the NIL8 cell at region B of Figure 9. The x-ray image resolves the edge structures from this region as well as internal voids that are difficult to visualize in the visible light micrograph.

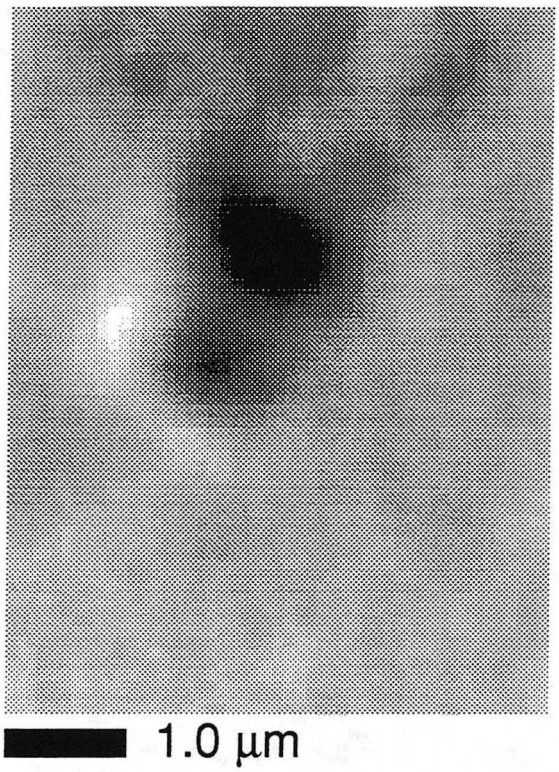

Visible light

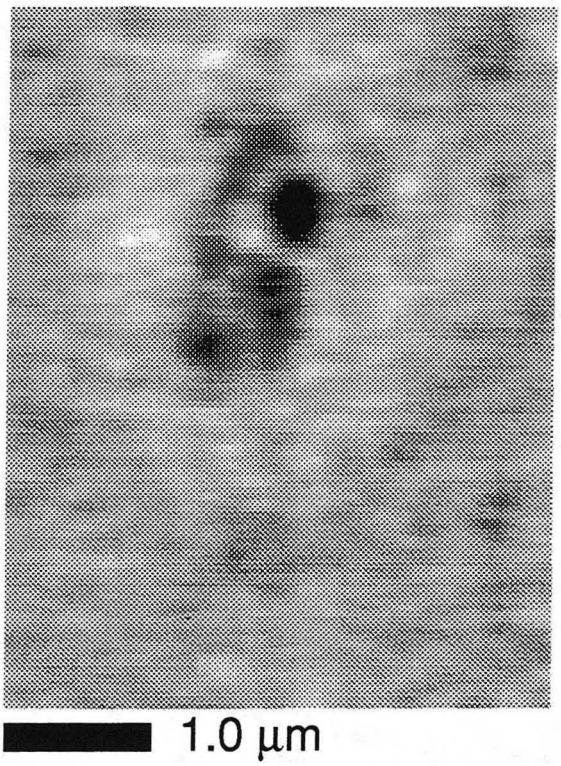

X-ray

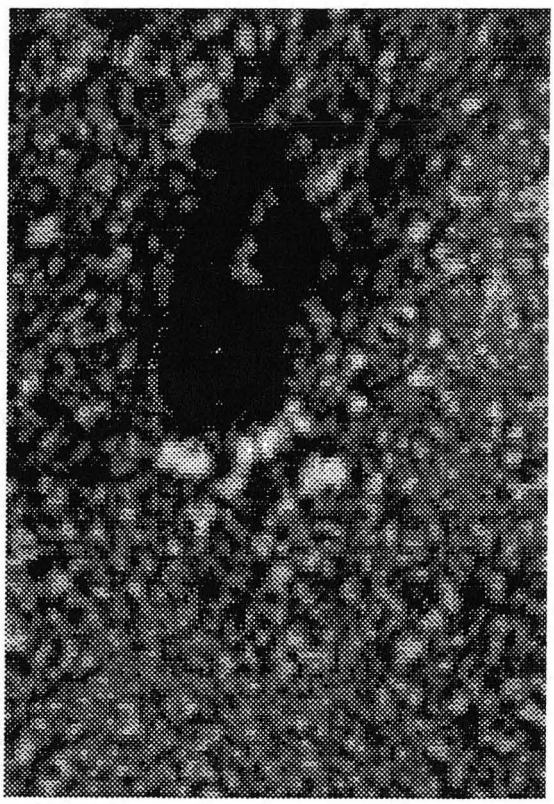

Electron

Figure 12: Visible light, x-ray holographic, and transmission electron micrographs of an organelle at region C in the middle of the NIL8 cell pseudopod of Figure 9. This area is well within the pseudopod in a region where the x-ray holographic technique should have trouble working well. However, the x-ray hologram reconstructs well and clearly shows structure not easily visualized in the visible light image.

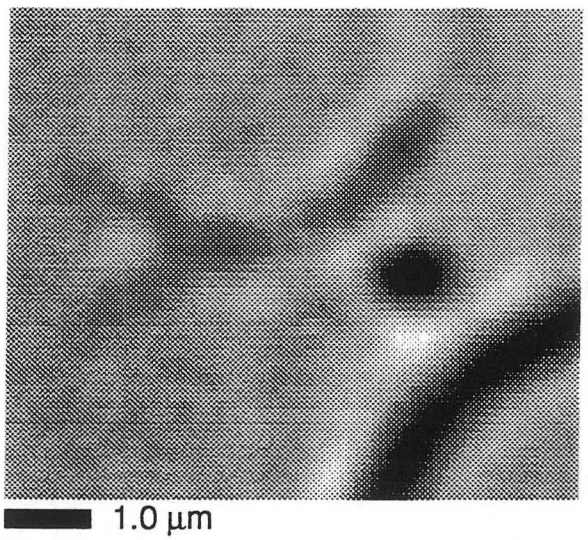

Visible light

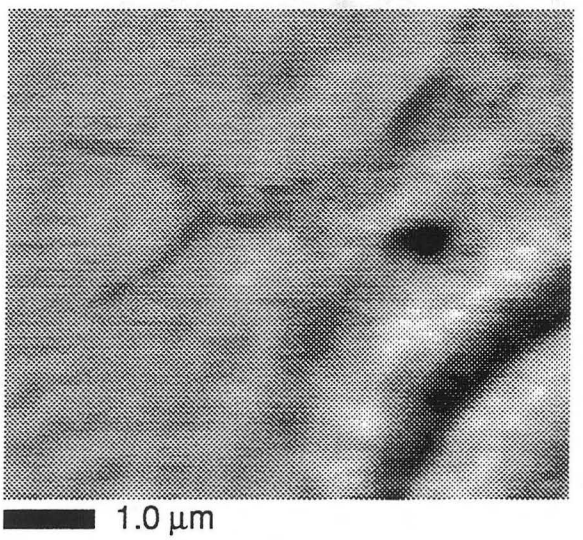

X-ray

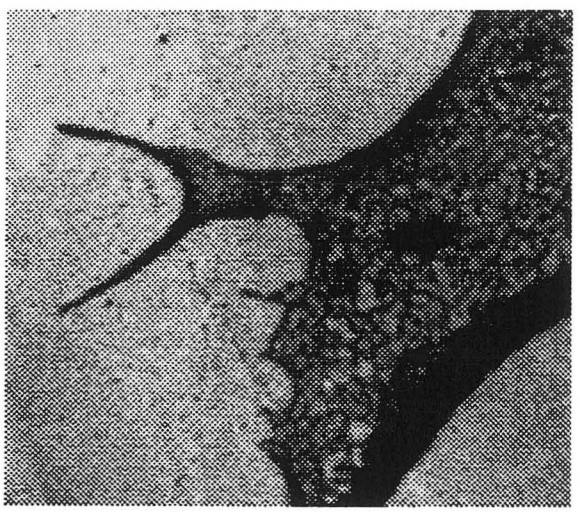

Electron

Figure 13: Visible light, x-ray holographic, and transmission electron micrographs of the edge of the NIL8 cell at region D of Figure 9.

holographic image are not artifacts. This validation of our x-ray holographic method is encouraging and leads us to consider its future potential in more detail.

10 Limitations on imaging due to radiation damage

Our broad intention for the future is to use holographic microscopy to image hydrated biological specimens. Ideally one would like to be able to image specimens in their natural wet state with resolution much higher than that of the light microscope and to make three-dimensional images by means of a tilt series with no limit on the number of exposures. Unfortunately, all of the currently-available high-resolution imaging methods that can collect three-dimensional information (other than surface topography) require the use of sufficiently penetrating ionizing radiation. This necessarily imposes limitations due to radiation damage.

The radiation dose required to form a sub-100 nm resolution, soft x-ray image using absorption contrast with even the most dose efficient technique is in the 10^4–10^5 Gray range [Sayre 1977, Kirz 1995]. Hydrated biological specimens at room temperature suffer mass loss and shrinkage at this dose level over time scales of seconds or longer even when they are chemically fixed [Williams 1993, Gilbert 1992]. These effects are due to reactions consequent upon the radiolysis of water. The detective quantum efficiency of the PMMA resists is thought to be about 10%, so that in our experiments radiation doses on the order of 10^6 Gray per hologram are required. Therefore, we cannot make even single holograms of natural hydrated samples without significant radiation damage. This is one reason why, for our present round of experiments, we have concentrated on the use of dehydrated specimens.

One might suppose that the dose required to make a tilt series of, say, N members would be N times greater than for a single two-dimensional image. However, it can be shown on information-theory grounds [Hegerl 1976, McEwen 1994] that the dose needed for definition of a single voxel with given statistical accuracy in a single view does not need to be increased if the voxel becomes part of a complex object and many views are taken so as to reconstruct the same voxel to the same statistical accuracy by tomographic methods. Some of the idealizations involved in arriving at this conclusion might be difficult to realize in a practical experiment but it suggests that something around 10^7 Gray may be required for a tomography experiment.

There are various strategies available to reduce radiation damage to wet specimens. One is the use of radical scavengers [Williams 1992]. These materials combine with the highly reactive free radicals formed by the radiolysis of water and reduce the rates of certain indirect forms of radiation damage. However, this approach does not prevent direct damage effects (*i.e.* ones not involving radicals) and so it cannot extend the damage resistance of natural biological material sufficiently to tolerate the 10^7 – Gray doses involved in high-resolution soft-x-ray tomography experiments.

A more effective approach is fixing and/or drying. These treatments lead to a considerable increase in radiation tolerance as reviewed for example by Kirz *et al.* [Kirz 1995]. However, resistance still does not extend to 10^7 Gray and various artifacts may be introduced.

It appears that the only way a hydrated sample can be made to tolerate the doses needed for x-ray-holographic tomography is by cooling it to liquid-nitrogen temperature. The electron-microscopy community have many years experience in imaging such cooled samples. One established technique is too cool the sample sufficiently rapidly (around $10^4\,^\circ$C/sec) so that the water in the sample forms amorphous ice. This type of ice gives good preservation of the interesting morphology

while slower freezing leads to the formation of ice crystals and consequent damage. The radiation hardness of biological samples at liquid-nitrogen temperature is such that 5 nm structural details survive at least until 10^8 Gray [Glaeser 1978].

We therefore conclude that high-resolution x-ray-holographic tomography *can* be implemented via cryofixation. Moreover, in view of the extensive experience already accumulated in doing cryo-electron microscopy, it seems that the practical difficulties are surmountable and that the increased penetration distance in water of soft x-rays versus electrons makes soft x-ray cryo-tomography uniquely suited for studying whole cell preparations.

11 Possibilities for better resolution

In order to improve image resolution we are making efforts on several fronts. One strategy is to record holograms at a reduced specimen-to-hologram distance z. This should enable the use of a smaller grid spacing, Δ_s,without needing a larger array size. In the longer term we will work toward better thermal stability of the AFM scanning stage (invar construction instead of aluminum) and an ability to process larger arrays. We are also studying ways to improve the signal-to-noise ratio of the recording. This could be based on reducing the PMMA noise by improved preparation and development techniques or on increasing the signal by an increase of the exposure. The prospects for improving the fundamental information-limited resolution are restricted by its very steep dependence on the dose. One can show [Aristov 1979, Howells 1988] that the dose varies inversely as the sixth power of the resolution. Thus once we reach a true limit to the resolution attainable at our present exposure levels, the additional improvement available by increasing the exposure will be something less than a factor of two.

12 Conclusion

In conclusion, we believe we have now demonstrated that soft-x-ray-holographic imaging utilizing atomic-force microscope readout is an approach which is capable of functioning for biological research. Furthermore, we believe that the way to enable both single and multiple x-ray-holographic imaging of hydrated biological material with minimal radiation and other artifacts is by imaging at cryogenic temperatures. We are constructing a new experimental system to be used initially at the X1A beam line at Brookhaven with capability for both cryoimaging and tilt series. We are optimistic that with this facility we will be able to obtain unique information in the regime of samples that are too thick for electron microscopy but possess interesting structures that are too small for observation in visible light.

13 Acknowledgments

We thank Ilan Spector for providing to us the NIL8 cell line, Vivian Oehler for maintaining and preparing the cell cultures, and Sue Wirick for assisting at the X1A beamline. This research was supported in part by the Alexander Hollaender Distinguished Postdoctral Fellowship Program (SL) sponsored by the Department of Energy, Office of Health and Environmental Research, and administered by the Oak Ridge Institute for Science and Education, the Department of Energy grant

DE-FG02-89ER60858, The National Science Foundation under grant BIR 91-12062, and Presidential Faculty Fellow award RCD 92-53618 (CJ). Holography experiments were carried out at the NSLS, which is supported by the U.S. Department of Energy.

14 References

[Aoki 1974] S. Aoki and S. Kikuta. X-ray holographic microscopy. *Japanese Journal of Applied Physics*, **13**, pp. 1385–1392, (1974).

[Aristov 1979] V. V. Aristov and G. A. Ivanova. On the possibility of utilizing holographic schemes in x-ray microscopy. *Journal of Applied Crystallography*, **12**, pp. 19–24, (1979).

[Aristov 1994] V. V. Aristov and A. I. Erko, editors. **X-ray Microscopy IV**, Chernogolovka, Moscow Region, (1994). Bogorodski Pechatnik.

[Baez 1952] A. V. Baez. A study in diffraction microscopy with special reference to x-rays. *Journal of the Optical Society of America*, **42**, pp. 756–762, (1952).

[Becker 1987] P. Becker, P. Seyfried, and H. Siegert. Translation stage for a scanning x-ray optical interferometer. *Review of Scientific Instruments*, **58**, pp. 207–211, (1987).

[Born 1980] M. Born and E. Wolf. **Principles of Optics**. Pergamon Press, Oxford, sixth edition, (1980).

[Browne 1992] M. T. Browne. Aspects of nanopositioning in stage design for scanning x-ray microscopes. In Michette et al. [Michette 1992], pp. 355–358.

[Collier 1971] R. J. Collier, C. B. Burckhardt, and L. H. Lin. **Optical Holography**. Academic Press, New York, (1971).

[El-Sum 1952] H. M. A. El-Sum. **Reconstructed wavefront microscopy**. PhD thesis, Stanford University, (1952).

[Fienup 1980] J. Fienup. Iterative method applied to image reconstruction and computer-generated holograms. *Optical Engineering*, **19**, pp. 297–305, (1980).

[Gabor 1948] D. Gabor. A new microscopic principle. *Nature*, **161**, pp. 777–778, (1948).

[Gerchberg 1972] R. Gerchberg and W. Saxton. A practical algorithm for the determination of phase from image and diffraction plane pictures. *Optik*, **35**, pp. 237–246, (1972).

[Gilbert 1992] J. R. Gilbert and J. Pine. Imaging and etching: soft x-ray microscopy on whole wet cells. In Jacobsen and Trebes [Jacobsen 1992b], pp. 402–408.

[Giles 1969] J. W. Giles, Jr. Image reconstruction from a Fraunhofer x-ray hologram with visible light. *Journal of the Optical Society of America*, **59**, pp. 1179–1188, (1969).

[Glaeser 1978] R. M. Glaeser and K. A. Taylor. Radiation damage relative to transmission electron microscopy of biological specimens at low temperature: a review. *Journal of Microscopy*, **112**, pp. 127–138, (1978).

[Goodman 1967] J. W. Goodman and R. W. Lawrence. Digital image formation from electronically detected holograms. *Applied Physics Letters*, **11**, pp. 77–79, (1967).

[Goodman 1968] J. W. Goodman. **An Introduction to Fourier Optics**. McGraw-Hill, San Francisco, (1968).

[Goodman 1985] J. W. Goodman. **Statistical Optics**. John Wiley & Sons, New York, (1985).

[Griffith 1994] J. E. Griffith, H. M. Marchman, and L. C. Hopkins. Edge position measurement with a scanning probe microscope. *Journal of Vacuum Science Technology*, **12**(6), pp. 3567–3570, (1994).

[Hawryluk 1975] R. J. Hawryluk, H. I. Smith, A. Soares, and A. M. Hawryluk. Energy dissipation in a thin polymer film by electron scattering: experiment. *Journal of Applied Physics*, **46**, pp. 2528–2537, (1975).

[Hegerl 1976] R. Hegerl and W. Hoppe. Influence of electron noise on three-dimensional image reconstruction. *Zeitschrift für Naturforschung*, **31 a**, pp. 1717–1721, (1976).

[Howells 1984] M. R. Howells. Possibilities for x-ray holography using synchrotron radiation. In G. Schmahl and D. Rudolph, editors, *X-ray Microscopy (Springer Series in Optical Sciences, Vol.* **43***)*, pp. 318–335, Berlin, (1984). Springer-Verlag.

[Howells 1986] M. R. Howells, M. A. Iarocci, and J. Kirz. Experiments in x-ray holographic microscopy using synchrotron radiation. *Journal of the Optical Society of America*, **A 3**, pp. 2171–2178, (1986).

[Howells 1987] M. Howells, C. Jacobsen, J. Kirz, R. Feder, K. McQuaid, and S. Rothman. X-ray holograms at improved resolution: a study of zymogen granules. *Science*, **238**, pp. 514–517, (1987).

[Howells 1988] M. R. Howells. Fundamental limits in x-ray holography. In Sayre et al. [Sayre 1988], pp. 263–271.

[Howells 1994] M. R. Howells and B. M. Kincaid. The properties of undulator radiation. In A. S. Schlachter and F. J. Wuilleumier, editors, *New Directions in Research with Third-Generation Soft X-ray Synchrotron Radiation Sources*, volume E 254, pp. 315–358. Kluwer Academic Publishers, London, (1994).

[Jacobsen 1988] C. Jacobsen, J. Kirz, M. Howells, R. Feder, D. Sayre, K. McQuaid, and S. Rothman. Progress in high resolution x-ray holographic microscopy. In Sayre et al. [Sayre 1988], pp. 253–262.

[Jacobsen 1990a] C. Jacobsen. X-ray holography: a history. In K. Shinohara, K. Yada, H. Kihara, and T. Saito, editors, *X-ray Microscopy in Biology and Medicine*, pp. 167–177, Berlin, (1990). Springer-Verlag. Also Japan Scientific Societies Press, Tokyo.

[Jacobsen 1990b] C. Jacobsen, M. Howells, J. Kirz, and S. Rothman. X-ray holographic microscopy using photoresists. *Journal of the Optical Society of America*, **A 7**, pp. 1847–1861, (1990).

[Jacobsen 1992a] C. Jacobsen, S. Lindaas, and M. Howells. X-ray holography using photoresists: high resolution lensless imaging. In Michette et al. [Michette 1992], pp. 244–250.

[Jacobsen 1992b] C. Jacobsen and J. Trebes, editors. **Soft X-ray Microscopy**, volume 1741, Bellingham, Washington, (1992). Society of Photo-Optical Instrumentation Engineers (SPIE).

[Jacobsen 1994] C. Jacobsen, E. Anderson, H. Chapman, J. Kirz, S. Lindaas, M. Rivers, S. Wang, S. Williams, S. Wirick, and X. Zhang. The X-1A scanning transmission x-ray microscope: Optics and instrumentation. In Aristov and Erko [Aristov 1994], pp. 304–321.

[Joyeux 1988a] D. Joyeux, S. Lowenthal, F. Polack, and A. Bernstein. X-ray microscopy by holography at LURE. In Sayre et al. [Sayre 1988], pp. 246–252.

[Joyeux 1988b] D. Joyeux and F. Polack. Progress in optical reconstruction of submicron x-ray holograms. In R. W. Falcone and J. Kirz, editors, *OSA Proceedings on Short Wavelength Coherent Radiation: Generation and Applications*, volume 2, pp. 295–302, Washington, D. C., (1988). Optical Society of America.

[Joyeux 1989a] D. Joyeux and F. Polack. 3-d in x-ray microscopy: Holography or classical imaging? *European J. Cell. Biol.*, **48 suppl. 25**, pp. 173–176, (1989).

[Joyeux 1989b] D. Joyeux, F. Polack, and R. Mercier. Principle of a 'reconstruction microscope' for high resolution x-ray holography. In R. Benattar, editor, *X-ray Instrumentation in Medicine and Biology, Plasma Physics, Astrophysics, and Synchrotron Radiation*, volume 1140, pp. 399–405, Bellingham, Washington, (1989). Society of Photo-Optical Instrumentation Engineers (SPIE).

[Kirz 1995] J. Kirz, C. Jacobsen, and M. Howells. Soft x-ray microscopy. *Quarterly Reviews of Biophysics*, **0**, (1995). Also available as Lawrence Berkeley Laboratory report LBL-36371.

[Koren 1993] G. Koren, F. Polack, and D. Joyeux. Iterative algorithms for twin-image elimination in in-line holography using finite-support constraints. *Journal of the Optical Society of America*, **A 10**, pp. 423–433, (1993).

[Leith 1962] E. N. Leith and J. Upatnieks. Reconstructed wavefronts and communication theory. *Journal of the Optical Society of America*, **52**, pp. 1123–1130, (1962).

[London 1989] R. A. London, M. D. Rosen, and J. E. Trebes. Wavelength choice for soft x-ray laser holography of biological samples. *Applied Optics*, **28**, pp. 3397–3404, (1989).

[London 1992] R. A. London, J. E. Trebes, and C. Jacobsen. Role of x-ray induced damage in biological microimaging. In Jacobsen and Trebes [Jacobsen 1992b], pp. 333–340.

[McEwen 1994] B. F. McEwen, K. H. Dowling, and R. M. Glaeser. The relevance of dose-fractionation in tomography of radiation-sensitive specimens. *The journal*, **0**, p. 0, (1994).

[McNulty 1992a] I. McNulty, J. Kirz, C. Jacobsen, E. Anderson, D. Kern, and M. Howells. High-resolution imaging by Fourier transform x-ray holography. *Science*, **256**, pp. 1009–1012, (1992).

[McNulty 1992b] I. McNulty, J. E. Trebes, J. M. Brase, T. J. Yorkey, R. Levesque, H. Szoke, E. H. Anderson, C. Jacobsen, and D. Kern. Experimental demonstration of high resolution three-dimensional x-ray holography. In Jacobsen and Trebes [Jacobsen 1992b], pp. 78–84.

[Michette 1986] A. G. Michette. **Optical Systems for Soft X Rays**. Plenum, New York, (1986).

[Michette 1988] A. G. Michette. X-ray microscopy. *Reports on Progress in Physics*, **51**, pp. 1525–1606, (1988).

[Michette 1992] A. G. Michette, G. R. Morrison, and C. J. Buckley, editors. **X-ray Microscopy III (Springer Series in Optical Sciences, Vol. 67)**, Berlin, (1992). Springer-Verlag.

[Mueller 1976] R. Mueller. X-ray laser applications study. Technical Report PD-LJ-76-132, Physical Dynamics, La Jolla, California, (1976). Section 7 of report edited by S. Jorna.

[Ochiai 1991] Y. Ochiai, M. Baba, H. Watanabe, and S. Matsui. Ten Nanometer Resolution Nanolithography using Newly Developed 50-kV Electron Beam Direct Writing System. *Jap. J. Appl. Phys.*, **30 B**, pp. 3266–3271, (November 1991).

[Queensgate] Queensgate. Instruments, (UK) Silwood Park, Ascot, Berkshire SL5 7PW England (0344) 872-317; (USA) 1760 Grand Avenue, Merrick, NY (516) 632-9725.

[Rarback 1990] H. Rarback, C. Buckley, H. Ade, F. Camilo, R. DiGennaro, S. Hellman, M. Howells, N. Iskander, C. Jacobsen, J. Kirz, S. Krinsky, S. Lindaas, I. McNulty, M. Oversluizen, S. Rothman, D. Sayre, M. Sharnoff, and D. Shu. Coherent radiation for x-ray imaging—the soft x-ray undulator and the X1A beamline at the NSLS. *Journal of X-ray Science and Technology*, **2**, pp. 274–296, (1990).

[Reuter 1976] B. Reuter and H. Mahr. Experiments with Fourier transform holograms using 4.48 nm x-rays. *Journal of Physics*, **E 9**, pp. 746–751, (1976).

[Rudolph 1990] D. Rudolph, G. Schmahl, and B. Niemann. Amplitude and phase contrast in x-ray microscopy. In P. J. Duke and A. G. Michette, editors, *Modern Microscopies*, pp. 59–67. Plenum, New York, (1990).

[Sarid 1991] D. Sarid. **Scanning Force Microscopy**. Oxford University Press, New York, (1991).

[Sayre 1977] D. Sayre, J. Kirz, R. Feder, D. M. Kim, and E. Spiller. Transmission microscopy of unmodified biological materials: Comparative radiation dosages with electrons and ultrasoft x-ray photons. *Ultramicroscopy*, **2**, pp. 337–341, (1977).

[Sayre 1988] D. Sayre, M. R. Howells, J. Kirz, and H. Rarback, editors. **X-ray Microscopy II (Springer Series in Optical Sciences, Vol. 56)**, Berlin, (1988). Springer-Verlag.

[Simpson 1983] M. J. Simpson and A. G. Michette. The effects of manufacturing inaccuracies on the imaging properties of Fresnel zone plates. *Optica Acta*, **30**, pp. 1455–1462, (1983). (now *Journal of Modern Optics*).

[Smith 1992] S. T. Smith and D. G. Chetwynd. **Foundations of Ultraprecision Mechanism Design**. Gordon and Breach Science Publishers, Reading, (1992).

[Solem 1982] J. C. Solem and G. C. Baldwin. Microholography of living organisms. *Science*, **218**, pp. 229–235, (1982).

[Solem 1986] J. C. Solem. Imaging biological specimens with high-intensity soft x rays. *Journal of the Optical Society of America*, **B 3**, pp. 1551–1565, (1986).

[Spiller 1976] E. Spiller, R. Feder, J. Topalian, D. Eastman, W. Gudat, and D. Sayre. X-ray microscopy of biological objects with Carbon Kα and with synchrotron radiation. *Science*, **191**, pp. 1172–1174, (1976).

[Stark 1987] H. Stark, editor. **Image Recovery: Theory and Application**. Academic Press Inc., New York, (1987).

[Stead 1992] A. D. Stead, R. A. Cotton, A. M. Page, M. D. Dooley, and T. W. Ford. Visualization of the effects of electron microscopy fixatives on the structure of hydrated epidermal hairs of tomato (*Lycopersicum peruvianum*) as revealed by soft x-ray contact microscopy. In Jacobsen and Trebes [Jacobsen 1992b], pp. 351–362.

[Stead 1995] A. D. Stead, R. A. Cotton, J. G. Duckett, J. A. Goode, A. M. Page, and T. W. Ford. The use of soft X rays to study the ultrastructure of living biological material. *Journal of X-ray Science and Technology*, **5**, pp. 52–64, (1995).

[Stroke 1964] G. W. Stroke and D. G. Falconer. Attainment of high resolutions in wavefront-reconstruction imaging. *Physics Letters*, **13**, pp. 306–309, (1964).

[Trebes 1987] J. E. Trebes, S. B. Brown, E. M. Campbell, D. L. Matthews, D. G. Nilson, G. F. Stone, and D. A. Whelan. Demonstration of x-ray holography with an x-ray laser. *Science*, **238**, pp. 517–519, (1987).

[Trebes 1992] J. Trebes, C. Annese, D. Birdsall, J. Brase, J. Gray, S. Lane, R. London, D. Matthews, D. Peters, D. Pinkel, G. Stone, D. Rapp, M. Rosen, U. Weier, and T. Yorkey. X-ray holography at Lawrence Livermore National Laboratory. In Michette et al. [Michette 1992], pp. 255–258.

[Tyler 1976] G. A. Tyler and B. J. Thompson. Fraunhofer holography applied to particle size analysis: a reassesment. *Optica Acta*, **23**, pp. 685–700, (1976).

[Williams 1992] S. P. Williams, C. J. Jacobsen, J. Kirz, X. Zhang, J. van't Hof, and S. Lamm. Radiation damage to chromosomes in the scanning transmission x-ray microscope. In Jacobsen and Trebes [Jacobsen 1992b], pp. 318–324.

[Williams 1993] S. Williams, X. Zhang, C. Jacobsen, J. Kirz, S. Lindaas, J. van't Hof, and S. S. Lamm. Measurements of wet metaphase chromosomes in the scanning transmission x-ray microscope. *Journal of Microscopy*, **170**, pp. 155–165, (1993).

[Zhang 1995] X. Zhang, C. Jacobsen, S. Lindaas, and S. Williams. Exposure strategies for PMMA from *in situ* XANES spectroscopy. *(to be published in J. Vac. Sci. Tech. B)*, (1995).

LAWRENCE BERKELEY NATIONAL LABORATORY
UNIVERSITY OF CALIFORNIA
TECHNICAL & ELECTRONIC INFORMATION DEPARTMENT
BERKELEY, CALIFORNIA 94720